REPORT DOCUMENTATION PAGE

Form Approved OMB NO. 0704-0188

1. REPORT DATE (DD-MM-YYYY)	2. REPORT TYPE	3. DATES COVERED (From - To)
09-02-2018	Final Report	1-Aug-2014 - 31-Dec-2017

4. TITLE AND SUBTITLE
Final Report: Millimeter Wave Mobile Ad Hoc Networks

5a. CONTRACT NUMBER
W911NF-14-1-0460

5b. GRANT NUMBER

5c. PROGRAM ELEMENT NUMBER
611102

6. AUTHORS

5d. PROJECT NUMBER

5e. TASK NUMBER

5f. WORK UNIT NUMBER

7. PERFORMING ORGANIZATION NAMES AND ADDRESSES

University of Texas at Austin
101 East 27th Street
Suite 5.300
Austin, TX 78712 -1532

8. PERFORMING ORGANIZATION REPORT NUMBER

9. SPONSORING/MONITORING AGENCY NAME(S) AND ADDRESS (ES)

U.S. Army Research Office
P.O. Box 12211
Research Triangle Park, NC 27709-2211

10. SPONSOR/MONITOR'S ACRONYM(S)
ARO

11. SPONSOR/MONITOR'S REPORT NUMBER(S)
65507-NS.31

12. DISTRIBUTION AVAILIBILITY STATEMENT

Approved for public release; distribution is unlimited.

13. SUPPLEMENTARY NOTES

The views, opinions and/or findings contained in this report are those of the author(s) and should not contrued as an official Department of the Army position, policy or decision, unless so designated by other documentation.

14. ABSTRACT

15. SUBJECT TERMS

16. SECURITY CLASSIFICATION OF:			17. LIMITATION OF ABSTRACT	15. NUMBER OF PAGES	19a. NAME OF RESPONSIBLE PERSON
a. REPORT	b. ABSTRACT	c. THIS PAGE			Robert Heath, Jr.
UU	UU	UU	UU		19b. TELEPHONE NUMBER 512-232-2014

RPPR Final Report
as of 19-Feb-2019

Agency Code:

Proposal Number: 65507NS **Agreement Number: W911NF-14-1-0460**
INVESTIGATOR(S):

Name: PhD Robert W Heath, Jr.
Email: rheath@mail.utexas.edu
Phone Number: 5122322014
Principal: Y

Organization: **University of Texas at Austin**
Address: 101 East 27th Street, Austin, TX 787121532
Country: USA
DUNS Number: 170230239 EIN: 746000203
Report Date: 30-Mar-2018 Date Received: 09-Feb-2018
Final Report for Period Beginning 01-Aug-2014 and Ending 31-Dec-2017
Title: Millimeter Wave Mobile Ad Hoc Networks
Begin Performance Period: 01-Aug-2014 **End Performance Period:** 31-Dec-2017
Report Term: 0-Other
Submitted By: PhD Robert Heath, Jr. Email: rheath@mail.utexas.edu
Phone: (512) 232-2014
Distribution Statement: 1-Approved for public release; distribution is unlimited.

STEM Degrees: 2 **STEM Participants:** 2

Major Goals: Major Goal 1: Wireless-power Transfer in mmWave Tactical Networks
In the previous years, we have developed an analytical framework for analyzing wireless power transfer in a mmWave ad hoc network with building blockages. A major goal this year is to characterize the performance of wireless power transfer in a mmWave tactical ad hoc network where RF power transmitters and energy harvesting receivers are (embedded into) wearable devices worn by soldiers. The nodes (i.e., soldiers) equipped with RF power transmitters remotely charge the ones equipped with energy harvesters. Because mmWave signals are susceptible to blockage by human-bodies, we evaluate the network-wide performance while incorporating the impact of blockages due to soldier bodies. Some of the key questions we seek to address are: how does the network density impact performance? What fraction of the network nodes be equipped with RF power transmitters to maximize the number of remotely-powered energy harvesting nodes? We used analysis and simulations to characterize the performance of this network in terms of system parameters such as network density, transmit power, energy harvesting parameters, blockage size, propagation conditions, and antenna array parameters. Our results suggest that network-level performance typically improves with an increase in the node density, despite an increase in blockages density.

Major Goal 2: Wireless-powered Communication Network with Short Packets
In the previous year, we developed an analytical frameowork for analyzing the performance of short packet wireless-powered communications in a three-node setup where an RF power transmitter remotely charges an energy harvesting node, which exploits the harvested energy to communicate data to another node. This year, we have extended the analysis to a large-scale network consisting of power transmitters, energy harvesting nodes, and their dedicated receiver nodes. Some of the key questions we seek to address include: how does the system parameters such as network density and transmit power impact performance? Is it beneficial to have a higher transmit power or a higher node density? How does the system perform in the short packet regime? We use analytical results and simulations to answer these questions.

Major Goal 3: Ergodic Rate of mmWave Ad Hoc Networks
The previous years developed frameworks to evaluate the ergodic rate of mmWave ad hoc networks with impairments such as beam alignment error. Using the developed framework the past year, we analyzed the training and beam alignment of mmWave ad hoc networks. We added the overhead of training to account for the degraded overall rate when accounting for the lost time for training. The results showed that, in contrast to cellular networks, the best strategy to align mmWave beams is to do an exhaustive search. Because the interference from

neighboring users can be high, directionality at the receiver and transmitter is required to reliably receive the training signals. Additionally, we investigated how the rate requirements of clustered users affects the communication between different clusters of users. The results showed that in order for clusters of users to stay connected between each other, the supported data rate must remain small.

Accomplishments: A summary of our accomplishments and detailed report is provided as a PDF document.

Training Opportunities: The project provided several opportunities for training and mentorship of graduate students. Two graduate students worked on this project. The first student was Andrew Thornburg. During the project, he developed his research skills. He solved important problems related to understanding the performance of millimeter wave networks including clustered ad hoc networks, beam training overhead, and the effects of mobility. His work established how and when millimeter wave is viable for tactical networks.
He also further developed his writing skills. The second student was Talha Khan. During his work on this project, he solved key challenges related to short packet communication and energy harvesting. In particular, he developed a compelling framework for incorporating the information theory based on short packets to make the analysis of energy harvesting networks more realistic. Energy harvesting has the potential to reduce the weight of batteries for soldiers. He also developed his writing and speaking skills.

Results Dissemination: The results of this research project have been disseminated through several complimentary venues during the past three years. Papers were presented at top conferences including MILCOM, GLOBECOM, ICC, and ICASSP. Journal papers were published in prestigious journals including the IEEE Transactions on Communications, the IEEE Transactions on Wireless Communications, the IEEE Transactions on Signal Processing, and IEEE Signal Processing Letters. Results were also incorporated into invited talks and plenaries. In addition, the results were presented at UT Austin during student poster sessions including at the Texas Wireless Summit, with 100-200 attendees. They were also presented to executives during the Wireless Networking and Communications Group annual board meeting, and the open house. Affiliates present include AT&T, CommScope, Crown Castle, General Dynamics, Huawei, National Instruments, Qualcomm, Samsung, Verizon, Yokogawa, Honda, and Toyota.

Honors and Awards: 2017 Fellow of the National Academy of Inventors

2017 European Association for Signal Processing (EURASIP) Technical Achievement Award

2017 IEEE ICC Best paper Award for the Signal Processing for Communications Symposium (with Wenqian Shen, Linglong DAi, Guan Gui, Zhaochen Wang, and Fumiyuki Adachi)

2017 IEEE Marconi Prize Paper Award in Wireless Communications (with Omar El Ayach, Sridhar Rajagopal, Shadi Abu-surra, and Zhouyue (Jerry) Pi)

IEEE GLOBECOM 2016 Most Attended Industry Panel Award (with Tom Marzetta)

Co-author of paper receiving the 2016 SPS Young Author Best Paper Award (given to my students Ahmed Alkhateeb and Omar El Ayach)

Named a Highly Cited Researcher 2015-2017 by Clarivate Analytics in Computer Science.

Protocol Activity Status:

Technology Transfer: The results of this research project were presented at UT Austin during student poster sessions including at the Texas Wireless Summit, with 100-200 attendees. They were also presented to executives during the Wireless Networking and Communications Group annual board meeting, and the UT Austin open house.

PARTICIPANTS:

Participant Type: PD/PI
Participant: Robert Wendell Heath Jr
Person Months Worked: 1.00 **Funding Support:**
Project Contribution:

International Collaboration:
International Travel:
National Academy Member: N
Other Collaborators:

Participant Type: Graduate Student (research assistant)
Participant: Andrew Thornburg
Person Months Worked: 9.00 **Funding Support:**
Project Contribution:
International Collaboration:
International Travel:
National Academy Member: N
Other Collaborators:

Participant Type: Graduate Student (research assistant)
Participant: Talha Khan
Person Months Worked: 9.00 **Funding Support:**
Project Contribution:
International Collaboration:
International Travel:
National Academy Member: N
Other Collaborators:

ARTICLES:

Publication Type: Journal Article Peer Reviewed: Y **Publication Status:** 4-Under Review
Journal: IEEE Transactions on Wireless Communications
Publication Identifier Type: Publication Identifier:
Volume: Issue: First Page #:
Date Submitted: 2/8/18 12:00AM Date Published: 2/8/18 6:00AM
Publication Location:
Article Title: Analysis of Mobility and Beamforming in mmWave Mobile Ad Hoc Networks
Authors: Andrew Thornburg, Robert W. Heath Jr.
Keywords: mmWave, ad hoc, beamforming
Abstract: Next-generation wireless devices using the large bandwidth at millimeter wave (mmWave) frequencies may exchange synchronization and training packets for proper alignment of antenna beams when communication is needed in order to focus energy. This overhead in training will reduce user perceived rates and increase latency in the network. In this paper, we develop design insights for mmWave ad hoc networks to minimize the delay and overhead. This paper uses stochastic geometry to define and compute metrics for expected data transmission delay due to synchronization and training and effective ergodic rate in mmWave ad hoc networks. The results indicate that for mmWave ad hoc networks, the antenna array size and transmission probability alter the optimality of the method used: in low interference or high array size regions, omni-directional reception reduces the training time. We define three network scenarios involving blockage to illustrate when each training method is best.
Distribution Statement: 1-Approved for public release; distribution is unlimited.
Acknowledged Federal Support: **Y**

RPPR Final Report
as of 19-Feb-2019

Publication Type: Journal Article Peer Reviewed: Y **Publication Status:** 0-Other
Journal: IEEE Transactions on Wireless Communications
Publication Identifier Type: DOI Publication Identifier: 10.1109/TWC.2016.2577582
Volume: 15 Issue: 9 First Page #: 6048
Date Submitted: 2/8/18 12:00AM Date Published: 9/1/16 12:00AM
Publication Location:
Article Title: Millimeter Wave Energy Harvesting
Authors: Talha Ahmed Khan, Ahmed Alkhateeb, Robert W. Heath
Keywords: millimeter wave, energy harvesting
Abstract: The millimeter wave (mmWave) band, a prime candidate for 5G cellular networks, seems attractive for wireless energy harvesting since it will feature large antenna arrays and extremely dense base station (BS) deployments. The viability of mmWave for energy harvesting though is unclear, due to the differences in propagation characteristics, such as extreme sensitivity to building blockages. This paper considers a scenario where low-power devices extract energy and/or information from the mmWave signals. Using stochastic geometry, analytical expressions are derived for the energy coverage probability, the average harvested power, and the overall (energy-and-information) coverage probability at a typical wireless-powered device in terms of the BS density, the antenna geometry parameters, and the channel parameters. Numerical results reveal several network and device level design insights.
Distribution Statement: 1-Approved for public release; distribution is unlimited.
Acknowledged Federal Support: **Y**

BOOKS:

Publication Type: Book Peer Reviewed: N **Publication Status:** 1-Published
Publication Identifier Type: ISBN Publication Identifier: 978-0134431796
Book Edition: 1 Volume: Publication Year: 2017 Date Received:
Publication Location:
Publisher: Prentice Hall
Book Title: Introduction to Wireless Digital Communication: A Signal Processing Perspective
Authors: Robert W. Heath Jr
Editor:
Acknowledged Federal Support: Y

CONFERENCE PAPERS:

Publication Type: Conference Paper or Presentation **Publication Status:** 1-Published
Conference Name: ICASSP 2015 - 2015 IEEE International Conference on Acoustics, Speech and Signal Processing (ICASSP)
Date Received: 30-Aug-2016 Conference Date: 18-Apr-2015 Date Published:
Conference Location: South Brisbane, Queensland, Australia
Paper Title: Interference statistics in a random mmWave ad hoc network
Authors: Andrew Thornburg, Tianyang Bai, Robert W. Heath
Acknowledged Federal Support: **Y**

Publication Type: Conference Paper or Presentation **Publication Status:** 1-Published
Conference Name: IEEE International Conference on Communications
Date Received: 30-Aug-2016 Conference Date: 08-Jun-2015 Date Published:
Conference Location: London, UK
Paper Title: MmWave Ad Hoc Network Coverage and Capacity
Authors: Andrew Thornburg, Tianyang Bai, Robert W. Heath
Acknowledged Federal Support: **Y**

RPPR Final Report
as of 19-Feb-2019

Publication Type: Conference Paper or Presentation **Publication Status:** 1-Published
Conference Name: MILCOM 2015 - 2015 IEEE Military Communications Conference
Date Received: 02-Sep-2017 Conference Date: 27-Oct-2015 Date Published:
Conference Location: Tampa, FL, USA
Paper Title: Ergodic capacity in mmWave ad hoc network with imperfect beam alignment
Authors: Andrew Thornburg, Robert W. Heath
Acknowledged Federal Support: **Y**

Publication Type: Conference Paper or Presentation **Publication Status:** 2-Awaiting Publicat
Conference Name: IEEE GLOBECOM Workshops
Date Received: 30-Aug-2016 Conference Date: 08-Dec-2016 Date Published: 30-Aug-2016
Conference Location: Washington DC, USA
Paper Title: On Wirelessly Powered Communications with Short Packets
Authors: Talha Ahmed Khan, Robert W. Heath Jr., Petar Popovski
Acknowledged Federal Support: **Y**

Publication Type: Conference Paper or Presentation **Publication Status:** 1-Published
Conference Name: IEEE GLOBECOM
Date Received: 08-Feb-2018 Conference Date: 05-Dec-2016 Date Published: 07-Feb-2017
Conference Location: Washington DC, USA
Paper Title: Capacity and Coverage in Clustered LOS mmWave Ad Hoc Networks
Authors: Andrew Thornburg, Robert W. Heath Jr.
Acknowledged Federal Support: **Y**

Publication Type: Conference Paper or Presentation **Publication Status:** 1-Published
Conference Name: MILCOM 2016 - 2016 IEEE Military Communications Conference (MILCOM)
Date Received: 02-Sep-2017 Conference Date: 01-Nov-2016 Date Published:
Conference Location: Baltimore, MD, USA
Paper Title: Capacity and scaling laws of dense mmWave and interference alignment ad hoc networks
Authors: Andrew Thornburg, Robert Heath, Robert Daniels
Acknowledged Federal Support: **Y**

Publication Type: Conference Paper or Presentation **Publication Status:** 1-Published
Conference Name: MILCOM 2017
Date Received: Conference Date: 23-Oct-2017 Date Published: 23-Oct-2017
Conference Location: Baltimore, MD
Paper Title: Analyzing Wireless Power Transfer in Millimeter Wave Networks with Human Blockages
Authors: Talha Khan, Robert Heath
Acknowledged Federal Support: **Y**

DISSERTATIONS:

Publication Type: Thesis or Dissertation
Institution: The University of Texas at Austin
Date Received: Completion Date: 12/1/17 5:20PM
Title: Analysis of Millimeter Wave Ad Hoc Networks
Authors: Andrew Thornburg
Acknowledged Federal Support: **Y**

RPPR Final Report
as of 19-Feb-2019

Publication Type: Thesis or Dissertation
Institution: The University of Texas at Austin
Date Received: Completion Date: 12/1/17 6:00AM
Title: Analysis and Design of Energy Harvesting Wireless Communication Systems
Authors: Talha Khan
Acknowledged Federal Support: **Y**

WEBSITES:

URL: http://www.profheath.org/research/millimeter-wave-cellular-systems/millimeter-wave-energy-harvesting/
Date Received: 31-Aug-2016
Title: Millimeter Wave Energy Harvesting
Description: Page that describes some of our results on energy harvesting
URL: http://www.profheath.org/research/millimeter-wave-cellular-systems/ad-hoc-mmwave-systems/
Date Received: 31-Aug-2016
Title: Millimeter Wave Ad Hoc Networks
Description: Research page linking our related work on millimeter wave ad hoc networks

Millimeter Wave Mobile Ad Hoc Networks Interim Progress Report

Robert W. Heath, Jr., Talha Khan, and Andrew Thornburg

CONTENTS

The authors are with the Department of Electrical and Computer Engineering, The University of Texas at Austin, Austin, TX 78712 USA (e-mail: rheath@ece.utexas.edu).

This work was supported by the Army Research Labs, Grant W911NF-14-1-0460.

I. Introduction

Millimeter wave (mmWave) communication will use high-bandwidth and directional antenna arrays to achieve truly next-generation data rates [2]–[4], [19], [59]. While the theoretical bit rate is incredible, which can allow the sharing of high-resolution video in a tactical military network or file sharing in a peer-to-peer network, several engineering hurdles remain. In previous generations, interference of nearby users limited performance of ad hoc networks. The properties of mmWave communication, however, offer opportunities to exploit the reduced interference created by directional antennas and building blockage.

While mmWave systems provide an enormous benefit in their bandwidth, there are several constraints that are not present in microwave systems. First, the mostly digital MIMO implementations found at microwave frequencies are unlikely; high-speed, high-bandwidth analog-digital converters require too much power to include many in a mobile device [61]. As a result, mmWave systems are more likely to use analog beamforming, or a hybrid approach [6], [22]. Second, mmWave propagation is much more sensitive to blockages than lower frequency signals [56]. While non-line-of-sight communication is possible, analysis should be aware of LOS / NLOS regimes as the path-loss exponent can be vastly different [60]. Third, mmWave devices will have dozens, perhaps hundred of antennas to overcome the path-loss. Historically, path loss has been viewed as a limiting factor for employing mmWave wireless systems; by fabricating many mmWave antennas in the same physical size of a single microwave antenna, the path-loss difference can be eliminated. These characteristics of mmWave mean that direct application of mmWave to MANETs without careful investigation is unwise.

In the first year of the project, we performed the following tasks related to capacity of outdoor mmWave ad hoc networks. We derive expressions for the transmission capacity of such networks. To derive the transmission capacity, we first obtain the SINR complimentary cumulative distribution function (CCDF) of an outdoor mmWave *ad hoc* network. We provide a bound on the CDF of the INR of a mmWave ad hoc network. We quantify the ergodic capacity of an outdoor mmWave ad hoc network. We use tools from stochastic geometry to derive an expression for the ergodic capacity that matches simulation results; the results are presented for both line-of-sight (LOS) and non-line-of-sight (NLOS) communication. We introduce and formalize the inevitable problem of beam misalignment in mmWave ad hoc networks and quantify the impact such errors have on the ergodic capacity of the network. We use a Gaussian antenna model; we contrast this with the sectored antenna model that has been widely used in the past. We present a simple expression that captures the loss of capacity for small alignment error.

In the second year of the project, we have investigated the ergodic capacity of tactical mmWave ad hoc networks. We derivate analytic solutions for uniform and cluster network topologies [71], [72]. We proposed scaling laws for mmWave ad hoc networks where the number of antennas at the transmitter and receiver scale sub-linearly with the transmitter density for constant per-user rate [69], [72]. We characterized the performance of a wireless-powered communication system where an RF energy harvesting node, charged by a power beacon via wireless energy transfer, attempts to communicate with a receiver over an AWGN channel [38]. Using the framework of finite-length information theory [48], we characterized the energy supply probability and the achievable rate of the considered system for the case of short packets. Leveraging the analytical results, we exposed the interplay between key system parameters such as the harvest and transmit blocklengths, the average harvested power, and the transmit power. We also provide closed-form analytical expressions for the asymptotically optimal transmit power.

In the third year of the project, we analyzed the system-level performance of mmWave wireless power transfer with human body blockages. This is important as wireless devices are getting smaller and more energy-efficient, wireless energy transfer is emerging as a potential technology for powering such low-power devices [73]. At the same time, in military sensor networks, where powering a potentially massive number of ad hoc devices will be a major challenge [82]. The mmWave band is attractive for wireless energy transfer as it allows deploying large antenna arrays in small form-factors. Unfortunately, the mmWave beams are susceptible to blockage by many common materials including human bodies [54]. We characterized the impact of human body blockages to determine when they are significant.

In the rest of this report, we provide prior work, a system model, and key results for the various problems studied during the past three years.

II. Capacity of mmWave Mobile Ad Hoc Networks

Lack of infrastructure characterize mobile ad hoc networks (MANETs). Whereas users in cellular networks only communicate with fixed base stations, users in MANETs communicate with each other; all users transmit, receive, or relay data. MANETs are particularly useful when infrastructure is destroyed by natural disasters or unavailable such as in a forward operating military network. Interference in the network limits the spatial density and efficiency of MANETs. Simple protocols create residual interference that leads to poor signal-to-interference-plus-noise ratios (SINRs) or try to coordinate transmissions leading to fewer transmission opportunities [9]. The purpose of this work is to investigate and optimize mmWave ad hoc networks as its characteristics enable fresh research problems in the area of ad hoc networks.

Modern wireless communication systems are interference limited meaning that unintended transmissions, e.g. other users, obfuscate the intended message. Newer cellular networks utilize sophisticated techniques to minimize interference. The less organized nature of ad-hoc networks lessens the opportunity to use these techniques. Many researchers proposed techniques to deal with interference in ad hoc networks. Seminal work in [29] shows that scaling of ad hoc networks goes by $1/\sqrt{n}$ where n is the number of users. Stochastic geometry has since become a favorite tool of researchers to attempt to improve the scaling of ad hoc networks. Transmission capacity is a popular information theoretic performance metric to assess the viability of *ad hoc* network architectures and transmissions strategies [9], [32], [33], [79]. The transmission capacity is the maximum spatial density of transmitters given an outage constraint [79] and is well studied, e.g. in [74], [75], [79], and references therein. The transmission capacity of *ad hoc* networks with directional antennas was computed in [33] assuming small-scale Rayleigh fading but neglecting large blockage effects. In mmWave systems, however, small-scale fading is not as severe as lower frequency systems and blockages effects are more significant [60]. In [74], the transmission capacity using MIMO beamforming for *ad hoc* networks was derived, where it was shown that the receive antennas should be used for interference cancellation not for spatial multiplexing. The ability to perform spatial interference cancellation, however, is limited as power-efficient hardware architectures limit mmWave devices often to simple directional beamforming [6]; each antenna on a mmWave device will likely not have a dedicated baseband hardware. Recent work has shown that mmWave systems are much less sensitive to interference due to the large directionality of mmWave arrays [62] and due to the likelihood of further interferers being blocked [13]. Therefore mmWave systems have the potential to offer larger amounts of spectrum while at the same time offer higher spectral efficiency due to reduced sensitivity to interference.

Beamforming and building blockage are defining characteristics of mmWave communication. Beamforming has been considered in *ad hoc* networks under the term *smart antennas*, phased

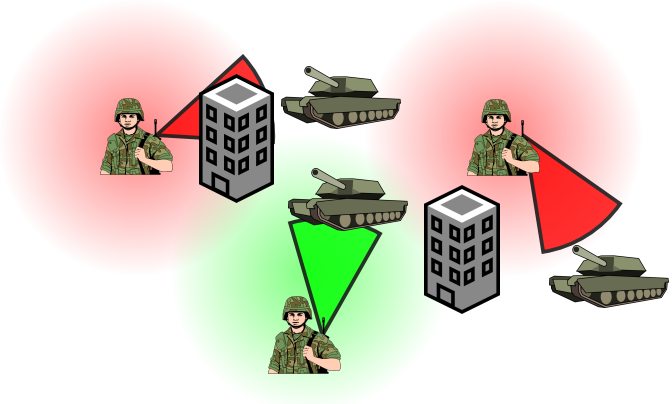

Fig. 1: MmWave networks direct the energy of transmission which reduces interference. Building blockage severely hinders mmWave propagation which further reduces interference.

arrays, or adaptive antennas. Prior work on *ad hoc* networks considered smart antennas and other directional antennas [18], [21], [51], [80]. A directional MAC testbed was benchmarked in [51]. In [18], the analysis and performance of the system assumes Rayleigh fading. The optimization of the MAC for directional antennas was discussed in [21], [80]. Current standards largely ignore adaptive beamforming at lower frequencies as the gains do not offset the overhead involved.

Together with beamforming, heavy signal blockage primarily dictates the performance of a mmWave network [17]. Building blockage has been incorporated into analysis previously [12], [26], [64]. A LOS-ball approach is taken in [64] for backhaul networks which is validated using real-world building data. In [26], link blockage results from small-scale fading. In our paper, link blockages due to obstacles like buildings which heavily attenuate mmWave signals [16]. The effect of blockage is developed in [17] for mmWave cellular networks; rate trends for cellular are captured with real-world building footprints in [41]. As illustrated in Fig. 1, the directionality of the array and building blockage limits the interference received.

A. *Stochastic Geometry Framework for Capacity Analysis*

The users in the ad hoc network are modeled as a homogeneous Poisson point process (PPP), Φ_{t} with intensity λ_{t}. In this process, the points, $x_i \in \Phi_{\mathrm{t}}$, are a transmitter with an associated receiver at a distance r away. The orientation of the receiver within the plane is a uniformly distributed mark, $\theta_i \in [0, 2\pi]$, on the PPP. Without loss of generality, we leverage Slivnyak's Theorem to analyze the *typical transmitter* located at the origin. Further, the *typical receiver* is located at $(r, 0)$.

Because of the physical propagation characteristics of mmWave, it is important to model large scale signal blockage (e.g. shadowing) [17], [60]. We model the blockage as in [16]. The center of buildings form another homogeneous PPP, Φ_b, on $\mathbb{R}^2$ with intensity λ_b. The length, width, and orientation of the buildings, L_i, W_i, ϕ_i, are independent marks on the building PPP each drawn from a distribution. It was shown in [16] that the probability that an *outdoor* user is LOS is exponentially decreasing dependent on the average building perimeter and the link distance, d. Specifically,

$$\mathbb{P}[\mathrm{LOS}|d = r] = e^{-\beta r} \tag{1}$$

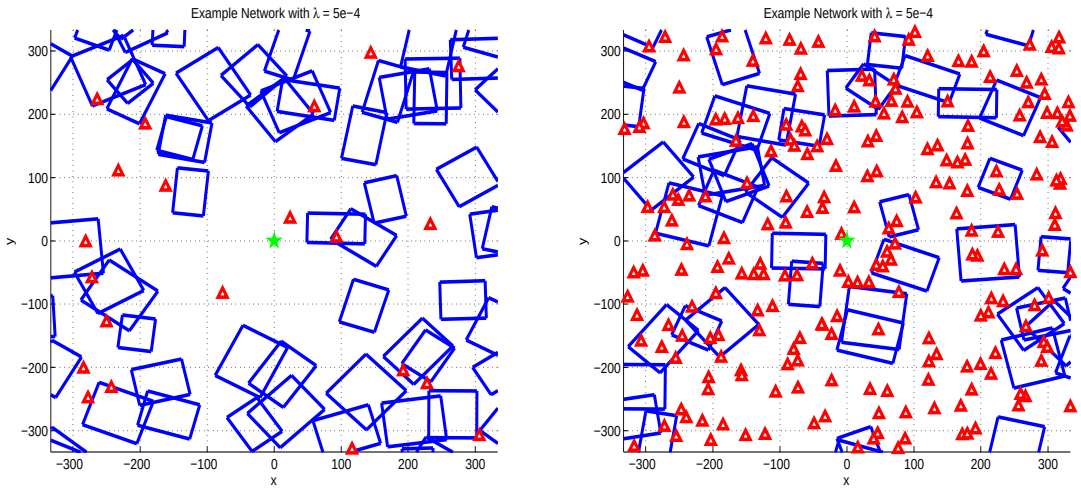

(a) (b)

Fig. 2: Example realizations of the random network with blockage. The blue rectangles are random boolean buildings which attenuate the signal. The red triangles are the Poisson point process of interferers. The green star represents the *typical node*.

with

$$\beta = \frac{2\lambda_{\mathrm{b}}(\mathbb{E}[W] + \mathbb{E}[L])}{\pi}, . \tag{2}$$

Examples of a realization of a mmWave ad hoc network with blockage are shown in Fig. 2. Measurements show that line-of-sight (LOS) and non-line-of-sight (NLOS) path-loss differ greatly in the path-loss exponent [14], [58]. We treat the path-loss exponent as a discrete random variable such that

$$\alpha_i = \begin{cases} \alpha_L & \text{w.p. } l_p(r) \\ \alpha_N & \text{w.p. } 1 - l_p(r) \end{cases}, \tag{3}$$

where α_L and α_N are the LOS and NLOS path-loss exponents and r is the link length. We set $l_p(r)$ to (1). Note that probability of the path-loss exponent is dependent on the blockage model. While we utilize [16], any arbitrary discrete probability mass function could be used.

Our work utilizes two antenna models that are popular in the literature: sectored and Gaussian [1], [14]. Fig. 3 shows the array gain for these two models. More precisely, we can define the gain of the sectored antenna as

$$G_i^{\mathrm{tx/rx}}(\theta) = \begin{cases} G & \theta \in [-\theta_{3dB}, \theta_{3dB}] \\ g & \text{otherwise} \end{cases}, \tag{4}$$

where θ is the angle-of-arrival/departure and the main lobe beamwidth is $2\theta_{3dB}$. We introduce the Gaussian antenna into the analysis of [70] which deals with antenna misalignment. If errors exist in the beam alignment, the sectored antenna will not capture the misalignment until the beams are *completely* misaligned. The Gaussian antenna provides a smoother roll-off and more accurately captures the antenna response of a uniform linear array or uniform circular array. The

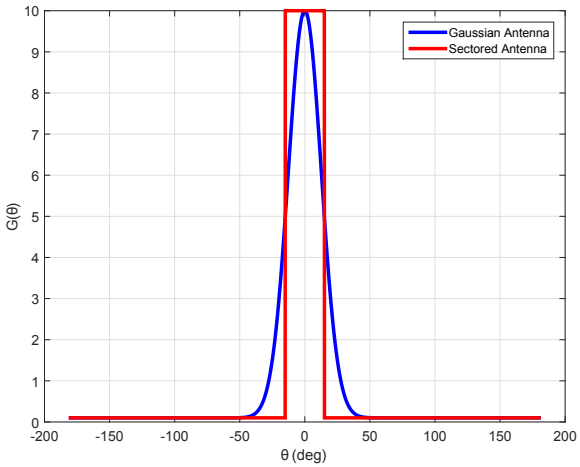

Fig. 3: A comparison of the antenna models used in the results. The sectored antenna is desirable due to its simplicity, but lacks a realistic roll-off in gain. In the Figure, each antenna has a beamwidth of 30° (e.g. $\theta_{3dB} = 15°$).

antenna response of a Gaussian antenna is

$$G_i^{\mathrm{tx/rx}}(\theta) = (G - g)e^{-\eta\theta^2} + g \tag{5}$$

where θ is the angle-of-arrival/departure, G is the maximum gain which occurs as $\theta = 0$, g is the side lobe gain, and η is a parameter that controls the 3dB beamwidth. We are interested in analyzing a *symmetric* ad hoc network where the transmitter and receiver have the same capabilities (e.g. antenna number).

We model the fading as a Nakagami random variable with parameter N_{h}. Consequently, the received signal power, h, can be modeled as a gamma random variable, $h \sim \Gamma(N_{\mathrm{h}}, 1/N_{\mathrm{h}})$. As $N_{\mathrm{h}} \to \infty$, the fading becomes a deterministic value centered on the mean, whereas $N_{\mathrm{h}} = 1$ corresponds to Rayleigh fading. A useful result for deriving the distributions of the SINR and INR will be a bound on the CDF of a gamma random variable. This was shown in [17] and refined in our work [66].

Lemma 1. *The cumulative distribution function of a normalized gamma random variable,* $y \sim \Gamma(k, 1/k)$*, can be tightly lower bounded as*

$$\left[1 - e^{-az}\right]^k < \mathbb{P}\left[y < z\right]$$

with $a = k(k!)^{-1/k}$.

The SINR is a key quantity that is central to our metrics. We define the SINR as

$$\mathrm{SINR}_0 = \frac{P_{\mathrm{t}} A G_0^{\mathrm{rx}} G_0^{\mathrm{tx}} h_0 r^{-\alpha_0}}{N_0 + \sum_{i \in \Phi_{\mathrm{t}}} P_{\mathrm{t}} A G_i^{\mathrm{rx}} G_i^{\mathrm{tx}} h_i d_i^{-\alpha_i}}, \tag{6}$$

where P_{t} is the transmit power of each users, $G^{\mathrm{rx/tx}}$ is the antenna gain of the receiver and transmitter (respectively), h_0 is the random fading power at the receiver of interest, A is the path-loss intercept, r is the fixed link length, α_i is the path-loss exponent, and N_0 is the noise power. The terms within the sum are for each interfering transmitter: d_i is used to represent the

distance from the interferer to receiver of interest, h_i is each interference random power, and $G^{\mathrm{rx/tx}}$ is the antenna gain of the interfering users. We similarly define the interference to noise ratio (INR) as

$$\mathrm{INR}_0 = \frac{\sum_{i\in\Phi_\mathrm{t}} P_\mathrm{t} A G_i^\mathrm{rx} G_i^\mathrm{tx} h_i d_i^{-\alpha_i}}{N_0}. \tag{7}$$

B. Key Results: SINR & INR Distributions

We define the CCDF of the SINR as

$$P_\mathrm{c}(T) = \mathbb{P}[\mathrm{SINR} \geq T], \tag{8}$$

where T is target SINR. In other works, (8) is referred to as the *coverage probability* [11], [33], [79]. We can use the law of total probability to expand the SINR CCDF as [17]

$$P_\mathrm{c}(T) = P_\mathrm{c}^\mathrm{L}(T)\mathbb{P}[\mathrm{LOS}] + P_\mathrm{c}^\mathrm{N}(T)\mathbb{P}[\mathrm{NLOS}], \tag{9}$$

where P_c^L and P_c^N are the conditional CCDFs on the event that the main link is LOS and NLOS, respectively. The SINR CCDF conditioned on the link being LOS is [17]

$$P_\mathrm{c}^\mathrm{L}(T) = \mathbb{P}[\mathrm{SINR} \geq T|\mathrm{LOS}]. \tag{10}$$

Going forward, for brevity, we will drop the conditional notation when using P_c^L. Using (6),

$$P_\mathrm{c}^\mathrm{L}(T) = \mathbb{P}\left[\frac{P_\mathrm{t} A G_0^\mathrm{rx} G_0^\mathrm{tx} h_0 r^{-\alpha_0}}{N_0 + \sum_{i\in\Phi_\mathrm{t}} P_\mathrm{t} A G_i^\mathrm{rx} G_i^\mathrm{tx} h_i d_i^{-\alpha_i}} \geq T\right] \tag{11}$$

$$= \mathbb{P}\left[h_0 \geq \frac{T r^{\alpha_\mathrm{L}}}{P_\mathrm{t} A G_0^\mathrm{rx} G_0^\mathrm{tx}}\left(N_0 + \sum_{i\in\Phi} \frac{P_\mathrm{t} A G_i^\mathrm{rx} G_i^\mathrm{tx} h_i}{d_i^{\alpha_i}}\right)\right] \tag{12}$$

$$= \mathbb{P}\left[h_0 \geq \frac{T r^{\alpha_\mathrm{L}}}{P_\mathrm{t} A G_0^\mathrm{rx} G_0^\mathrm{tx}}(N_0 + I_\Phi)\right] \tag{13}$$

$$= 1 - \mathbb{P}\left[h_0 < \frac{T r^{\alpha_\mathrm{L}}}{P_\mathrm{t} A G_0^\mathrm{rx} G_0^\mathrm{tx}}(N_0 + I_\Phi)\right] \tag{14}$$

$$= 1 - \int_0^\infty \mathbb{P}\left[h_0 < \frac{T r^{\alpha_\mathrm{L}}}{P_\mathrm{t} A G_0^\mathrm{rx} G_0^\mathrm{tx}}(N_0 + x)|I_\Phi = x\right] p_\Phi(x) dx. \tag{15}$$

Now we can bound (15) with $h_0 \sim \Gamma(N_\mathrm{h}, 1/N_\mathrm{h})$ as

$$P_\mathrm{c}^\mathrm{L}(T) < 1 - \int_0^\infty \left[\left(1 - e^{-a\frac{T r^{\alpha_\mathrm{L}}}{P_\mathrm{t} A G_0^\mathrm{rx} G_0^\mathrm{tx}}(N_0+x)}\right)^{N_\mathrm{h}}\right] p_\Phi(x) dx \tag{16}$$

$$< 1 - \mathbb{E}_\Phi\left[\left(1 - e^{-a\frac{T r^{\alpha_\mathrm{L}}}{P_\mathrm{t} A G_0^\mathrm{rx} G_0^\mathrm{tx}}(N_0+I_\Phi)}\right)^{N_\mathrm{h}}\right] \tag{17}$$

$$= \sum_{n=1}^{N_\mathrm{h}} \binom{N_\mathrm{h}}{n} (-1)^{n+1} \mathbb{E}_\Phi\left[e^{-an\frac{T r^{\alpha_\mathrm{L}}}{P_\mathrm{t} A G_0^\mathrm{rx} G_0^\mathrm{tx}}(N_0+I_\Phi)}\right], \tag{18}$$

where (18) is from the Binomial Theorem [17].

Because each building blockage is independent, we use the Thinning Theorem from stochastic geometry [10]. The antenna array gain of each interfering user is also independent which allows us to thin the PPP. We use the sectored antenna model in this work which constrains the gain

to three values ($\{GG, Gg, gg\}$). Essentially, we can now view the interference as 6 independent PPPs such that

$$I_{\Phi} = I^{GG}_{\Phi_{\mathrm{LOS}}} + I^{Gg}_{\Phi_{\mathrm{LOS}}} + I^{gg}_{\Phi_{\mathrm{LOS}}} + I^{GG}_{\Phi_{\mathrm{NLOS}}} + I^{Gg}_{\Phi_{\mathrm{NLOS}}} + I^{gg}_{\Phi_{\mathrm{NLOS}}}, \tag{19}$$

with the superscripts representing the discrete random antenna gain defined in (4) and each interfering node either a LOS transmitter or NLOS transmitter. Because of this, we can distribute the expectation in (18) and re-write (18) as

$$P^{\mathrm{L}}_{\mathrm{c}} < \sum_{n=1}^{N_{\mathrm{h}}} (-1)^{n+1} \binom{N_{\mathrm{h}}}{n} e^{-nK_{\mathrm{L}}TN_0} \prod_i \prod_j \mathbb{E}_{I_{\Phi^i_j}} \left[e^{-nK_{\mathrm{L}}TI_{\Phi^i_j}} \right] \tag{20}$$

with $i \in \{GG, Gg, gg\}$, $j \in \{\mathrm{LOS}, \mathrm{NLOS}\}$, and $K_{\mathrm{L}} = \frac{ar^{\alpha_{\mathrm{L}}}}{P_{\mathrm{t}} A G_0^{\mathrm{rx}} G_0^{\mathrm{tx}}}$. In (20), i and j index each interference sub-PPP. In essence, each expectation is the Laplace transform of the associated sub-PPP, and each of these Laplace transforms are multiplied together.

Using stochastic geometry theory, we can analytically represent the first Laplace expectation term as

$$\mathbb{E}\left[e^{-nK_{\mathrm{L}}TI^{GG}_{\Phi_{\mathrm{LOS}}}} \right] = e^{-2\pi\lambda p_{GG} \int_0^{\infty} \left(1 - \mathbb{E}_h \left[e^{-\frac{nK_{\mathrm{L}}TP_{\mathrm{t}}AGGh}{x^{\alpha_{\mathrm{L}}}}} \right] \right) l_p(x) x \mathrm{d}x}. \tag{21}$$

The probability of gain GG and LOS probabilities, p_{GG} and $l_p(r)$, capture the thinning of the PPP for the first sub-PPP in (19). Notice that $\mathbb{E}_h[e^{\eta h}]$ corresponds to the moment-generating function (MGF) of the random variable h, which is modeled as a gamma random variable with parameter N_{h} which has a known MGF. A similar approach was taken in [17] for the analysis of mmWave cellular networks. The final Laplace transform of the PPP is given as

$$\mathcal{L}_{I^{GG}_{\Phi_{\mathrm{LOS}}}} = e^{-2\pi\lambda p_{GG} \int_0^{\infty} \left(1 - 1/(1 + \frac{nQ_{\mathrm{L}}T}{x^{\alpha_{\mathrm{L}}} N_{\mathrm{h}}})^{N_{\mathrm{h}}} \right) l_p(x) x \mathrm{d}x}. \tag{22}$$

with $Q_{\mathrm{L}} = K_{\mathrm{L}} P_{\mathrm{t}} GGA = ar^{\alpha_{\mathrm{L}}}$. Each other Laplace transform is computed similarly, but noting that p_{GG}, $l_p(r)$, and $x^{\alpha_{\mathrm{L}}}$ will change depending on the antenna gain of the sub-PPP and if the sub-PPP is LOS or NLOS. We can summarize the results in the following theorem

Theorem 1. *The SINR distribution of an outdoor mmWave* ad hoc *network can be tightly upper bounded by*

$$\begin{aligned} P_{\mathrm{c}}(T) < & \sum_{n=1}^{N_{\mathrm{h}}} \binom{N_{\mathrm{h}}}{n} (-1)^{n+1} e^{-nK_{\mathrm{L}}TN_0} e^{-2\pi\lambda(V+Y)} l_p(r) + \\ & \sum_{n=1}^{N_{\mathrm{h}}} \binom{N_{\mathrm{h}}}{n} (-1)^{n+1} e^{-nK_{\mathrm{N}}TN_0} e^{-2\pi\lambda(W+Z)} \Big(1 - l_p(r) \Big) \end{aligned} \tag{23}$$

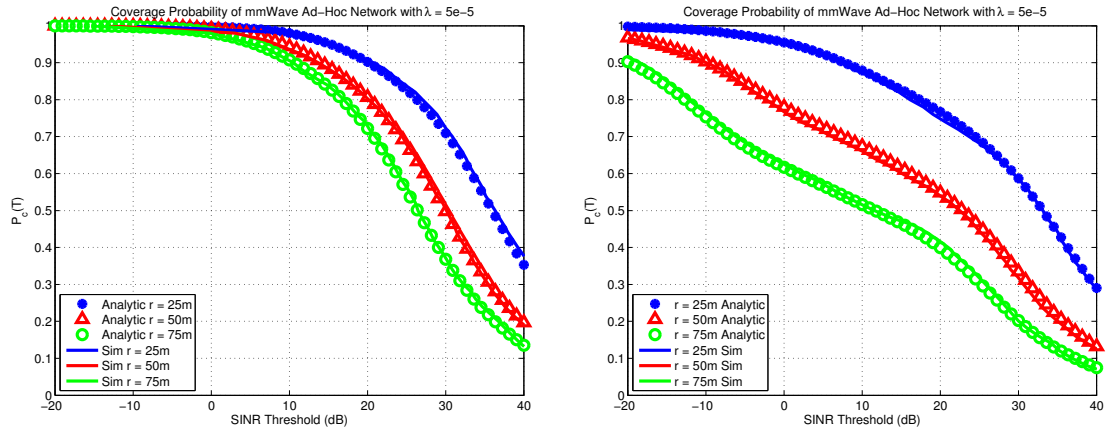

(a) (b)

Fig. 4: The SINR distribution of mmWave *ad hoc* networks with $\lambda = 5\times10^{-5}$. In (a), we assume LOS communication only whereas in (b) both LOS and NLOS communication is permitted.

where

$$V = \sum_i p_i \int_0^\infty \left[1 - 1/\left(1 + \frac{nQ_{\mathrm{L}}T}{x^{\alpha_{\mathrm{L}}}N_{\mathrm{h}}}\right)^{N_{\mathrm{h}}}\right] l_p(x)x\mathrm{d}x \tag{24}$$

$$Y = \sum_i p_i \int_0^\infty \left[1 - 1/\left(1 + \frac{nQ_{\mathrm{L}}T}{x^{\alpha_{\mathrm{L}}}N_{\mathrm{h}}}\right)^{N_{\mathrm{h}}}\right] \big(1 - l_p(x)\big)x\mathrm{d}x \tag{25}$$

$$W = \sum_i p_i \int_0^\infty \left[1 - 1/\left(1 + \frac{nQ_{\mathrm{N}}T}{x^{\alpha_{\mathrm{N}}}N_{\mathrm{h}}}\right)^{N_{\mathrm{h}}}\right] l_p(x)x\mathrm{d}x \tag{26}$$

$$Z = \sum_i p_i \int_0^\infty \left[1 - 1/\left(1 + \frac{nQ_{\mathrm{N}}T}{x^{\alpha_{\mathrm{N}}}N_{\mathrm{h}}}\right)^{N_{\mathrm{h}}}\right] \big(1 - l_p(x)\big)x\mathrm{d}x \tag{27}$$

with $K_{\mathrm{L}} = \frac{ar^{\alpha_{\mathrm{L}}}}{P_{\mathrm{t}}AG_0^{\mathrm{rx}}G_0^{\mathrm{tx}}}$, $K_{\mathrm{N}} = \frac{ar^{\alpha_{\mathrm{N}}}}{P_{\mathrm{t}}AG_0^{\mathrm{rx}}G_0^{\mathrm{tx}}}$, $G_i \in \{GG, Gg, gg\}$, $Q_{\mathrm{L}} = \frac{ar^{\alpha_{\mathrm{L}}}G_i}{G_0^{\mathrm{rx}}G_0^{\mathrm{tx}}}$, *and* $Q_{\mathrm{N}} = \frac{ar^{\alpha_{\mathrm{N}}}G_i}{G_0^{\mathrm{rx}}G_0^{\mathrm{tx}}}$.

Figure 4 shows the SINR CCDF for a mmWave network of user density $\lambda = 5 \times 10^{-5}$ with building parameter $\beta = 0.008$ which corresponds to the UT Austin building footprint. These results show the validation of Theorem 1 as well as motivate a LOS aware protocol. Especially for larger link distances, Fig. 4b shows much less favorable SINR than 4a. If the user density is high enough, we believe that using relays in the ad hoc network will add capacity to the network.

We are interested in the transition from noise-limited to interference-limited operation as a function of user density, building density, antenna pattern, and transmission distance. The transition between noise-limited and interference-limited is very important to algorithm and protocol design. We achieve this by characterizing the INR CDF. We define the INR CDF as

$$P^{\mathrm{NL}}(T) = \mathbb{P}[\mathrm{INR} \leq T]\text{..} \tag{28}$$

We prove the following theorem in a similar way. Most of the derivation will be omitted for

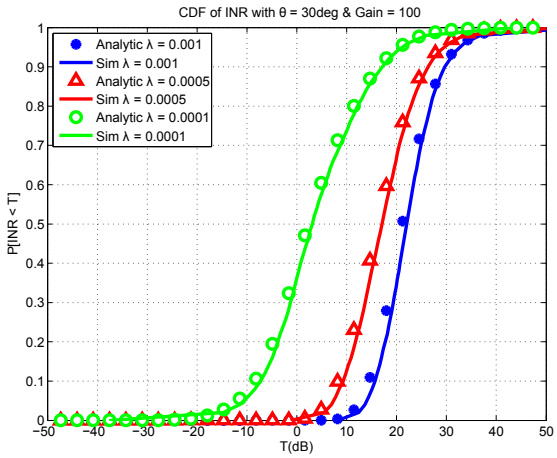

Fig. 5: The INR CDF for $\theta = 30°$. In the sparsest network, the interference power is more dominant than the noise power (i.e. $\mathbb{P}[\mathrm{INR} < 0\mathrm{dB}] = 0.4$ for the green circle network), but the red triangle curve shows that the network is always interference limited.

brevity, but call attention to N_{C}. After some manipulation of the INR expression, we arrive at

$$P^{\mathrm{NL}}(T) \;\; = \;\; 1 - \mathbb{P}\left[1 < \frac{I_{\Phi}}{TN_0}\right]. \tag{29}$$

To analytically evaluate $\mathbb{P}\left[1 < \frac{I_{\Phi}}{TN_0}\right]$, replace 1 with a random variable, C, with low variance. We let $C \sim \Gamma(N_{\mathrm{C}}, 1/N_{\mathrm{C}})$. We bound the low-variance gamma random variable in the same manner as the SINR derivation to arrive at Theorem 2.

Theorem 2. *The* INR *distribution of a mmWave* ad hoc *network can be tightly bounded by*

$$P^{\mathrm{NL}}(T) < \sum_{n=1}^{N_{\mathrm{C}}} \binom{N_{\mathrm{C}}}{n} (-1)^{n+1} e^{-2\pi\lambda(R+U)} \tag{30}$$

where

$$R = \sum_i p_i \int_0^{\infty} \left(1 - 1/\big(1 + \frac{anG_i^{\mathrm{rx}}G_i^{\mathrm{tx}}}{x_{\mathrm{L}}^{\alpha} N_0 T N_{\mathrm{h}}}\big)^{N_{\mathrm{h}}}\right) l_p(x) x \mathrm{d}x \tag{31}$$

$$U = \sum_i p_i \int_0^{\infty} \left(1 - 1/\big(1 + \frac{anG_i^{\mathrm{rx}}G_i^{\mathrm{tx}}}{x_{\mathrm{N}}^{\alpha} N_0 T N_{\mathrm{h}}}\big)^{N_{\mathrm{h}}}\right) \big(1 - l_p(x)\big) x \mathrm{d}x \tag{32}$$

with $i \in \{GG, Gg, gg\}$.

In Fig. 5, we show the INR for networks with 100, 500, and 1000 users per km^2 with antenna beamwidths of $30°$. Indeed, the sparsest network exhibits noise limited behavior. For example, the $\mathbb{P}[\mathrm{INR} < 0\mathrm{dB}] = 0.4$ for $30°$ antennas in the sparest network. Yet, these results show compelling evidence that a mmWave ad hoc network can still be considered interference limited. In dense networks (500 and 1000 users per km^2), the network exhibits strong interference. Because of this, we urge caution when considering mmWave networks to be noise limited.

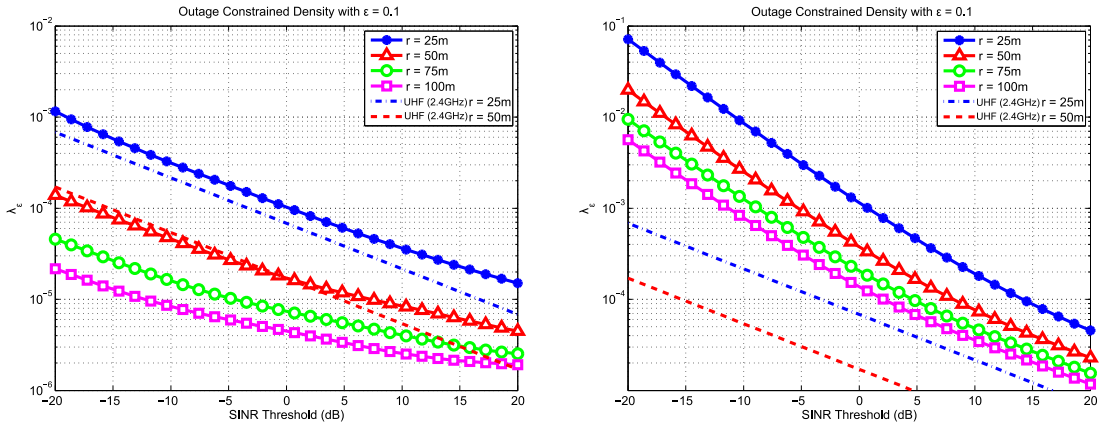

(a) (b)

Fig. 6: The largest λ for a 10% outage at various SINR thresholds and dipole distances for NLOS/LOS communication (a) and LOS-only communication (b). Note the different y-axis scales.

C. Key Results: Transmission Capacity

Now, using Theorem 1, we characterize the transmission capacity, λ_ϵ. This is the largest λ the network can support given an SINR threshold, T and outage ϵ. More simply, $1-\epsilon = P_{\mathrm{c}}$ of users will have an SINR larger than T. It can also be defined as the number of successful transmissions per unit area, which is directly connected to the number of users supported by the network. To do this, we approximate the exponential terms of Theorem 1 as

$$P_{\mathrm{c}}^{\mathrm{L}} < \sum_{n=1}^{N_{\mathrm{h}}} (-1)^{n+1} \binom{N_{\mathrm{h}}}{n} e^{-nK_{\mathrm{L}}TN_0} \left(1 - 2\pi\lambda_\epsilon \Theta + 2\pi\lambda_\epsilon^2 \Theta^2\right) \tag{33}$$

where $\Theta = V + Y$. We leverage the bound, $e^{-x} \leq (1 - x + x^2/2)$ for $x \in \mathbb{R}^+$, for the Laplace functional term. This bound is tight for small x. We are interested in analyzing the optimal λ for P_{c} near 1. As a result, the Laplace functional will be close to 1; the argument will be close to 0. A similar bound is done for the NLOS term in Theorem 1. We combine (33) and the NLOS approximation to form

$$\begin{aligned} 1-\epsilon < &\sum_{n=1}^{N_{\mathrm{h}}} (-1)^{n+1} \binom{N_{\mathrm{h}}}{n} e^{-nK_{\mathrm{L}}TN_0} \left(1 - 2\pi\lambda_\epsilon \Theta + 2\pi\lambda_\epsilon^2 \Theta^2\right) + \\ &\sum_{n=1}^{N_{\mathrm{h}}} (-1)^{n+1} \binom{N_{\mathrm{h}}}{n} e^{-nK_{\mathrm{N}}TN_0} \left(1 - 2\pi\lambda_\epsilon \Psi + 2\pi\lambda_\epsilon^2 \Psi^2\right) \end{aligned} \tag{34}$$

with $\Psi = W + Z$. Because of this bound, P_{c} is now a quadratic equation in λ which can be solved in closed-form. The exact solution depends on N_{h}. Symbolic tools, such as *Mathematica*, can factor and solve (34) such that

$$\lambda_\epsilon = f(T, \epsilon). \tag{35}$$

Fig. 6 shows the transmission capacity for mmWave and lower frequency networks with a 10% outage. Fig. 6 shows the relationship between providing a higher SINR (and thus rate) to

users while maintaining a constant outage constraint. As expected, the shortest dipole length can support the highest density of users. A linear increase in SINR (in dB) results in an exponential decrease in the density of users in the network. We include a comparison with lower frequency *ad hoc* networks [11].

In Fig. 6a, both LOS and NLOS communication is allowed. If the dipole length is 25m, mmWave networks can allow a larger density. If the dipole length is 50m, however, lower-frequency networks can permit higher densities if the SINR threshold is lower. Fig. 6b shows the improvement if communication is kept to LOS links. The mmWave network in Fig. 6b can support an order-of-magnitude more users than the network in Fig. 6a. Furthermore, a vast improvement over lower-frequency networks is shown. If users require SINR $>$ 0dB 90% of the time, 25m link length can support networks with $d_n = 15$m ($\lambda = 10^{-3}\text{m}^{-2}$) whereas lower frequency networks require a neighbor distance of 50m ($\lambda = 10^{-4}\text{m}^{-2}$).

1) Ergodic Capacity with Misalignment: We define the ergodic capacity as the average sum spectral efficiency per unit area of the network.

$$C = \mathbb{E}\left[\sum_{i\in\Phi_{\text{t}}} \log_2\left(1+\text{SINR}_i\right)\right] \tag{36}$$

$$\overset{(a)}{=} \lambda\mathbb{E}\left[\log_2\left(1+\text{SINR}_0\right)\right], \tag{37}$$

with Φ being the PPP of users with intensity λ, and (a) is due to Slivnyak's Theorem where we analyze the *typical* user located at the origin [10]. We leverage the following lemma from [42] to evaluate the ergodic capacity of a mmWave ad hoc network.

Lemma 2. *Let $X > 0$ and $Y > 0$ be non-negative and independent random variables. Then, for any $a > 0$,*

$$\mathbb{E}\left[\ln\left(1+\frac{X}{a+Y}\right)\right] = \int_0^\infty \frac{e^{-az}}{z}\left(1-\mathbb{E}\left[e^{-zX}\right]\right)\mathbb{E}\left[e^{-zY}\right]dz. \tag{38}$$

By performing a change of logarithms, Lemma 2 allows the evaluation of (37). Notice that $\mathbb{E}[e^{-zX}]$ is the moment-generating function of X which is the denominator of the SINR. The final term, $\mathbb{E}[e^{-zY}]$, is the Laplace transform of the interference which was computed previously for the SINR CCDF. Thus, we can summarize the results in the following theorem.

Theorem 3. *The ergodic capacity per unit area (bits/sec/Hz/m^2) of an outdoor mmWave network is*

$$C = \frac{\lambda}{\ln(2)}\int_0^\infty \frac{e^{-zN_0-2\pi\lambda(V+W)}}{z}\left(1-S\right)dz \tag{39}$$

with

$$
\begin{aligned}
S =& p(r)\left(1+\frac{zAP_{\mathrm{t}}G_0^{\mathrm{tx}}G_0^{\mathrm{rx}}}{r^{\alpha_L}N_h}\right)^{-N_h}+(1-p(r))\left(1+\frac{zAP_{\mathrm{t}}G_0^{\mathrm{tx}}G_0^{\mathrm{rx}}}{r^{\alpha_N}N_h}\right)^{-N_h}\\
V =& \sum_i p_i\int_0^\infty\left[1-1/\left(1+\frac{zAP_{\mathrm{t}}G_i^{\mathrm{tx}}G_i^{\mathrm{rx}}}{x^{\alpha_L}N_h}\right)^{N_h}\right]p(x)x\mathrm{d}x\\
W =& \sum_i p_i\int_0^\infty\left[1-1/\left(1+\frac{zAP_{\mathrm{t}}G_i^{\mathrm{tx}}G_i^{\mathrm{rx}}}{x^{\alpha_N}N_h}\right)^{N_h}\right](1-p(x))\,x\mathrm{d}x.
\end{aligned}
$$

Theorem 3 assumes that the desired signal is always properly aligned. If the antenna arrays are not perfectly aligned, the signal strength will degrade which results in a loss of capacity. We model the alignment error as $\epsilon \sim \mathcal{N}_T(0,\sigma^2)$ where $\mathcal{N}_T$ is the truncated Gaussian distribution and σ^2 is the variance of the error. The Cramer-Rao bound gives a lower bound on the variance of the error [52], [65].

In the following lemmas, we note that in high SINR (37) can be approximated as

$$
C \;\approx\; \lambda\mathbb{E}\left[\log_2\left(\mathrm{SINR}_0\right)\right]. \tag{40}
$$

Additionally, we note that because of the isotropic properties of the PPP, the interference statistics will be invariant with antenna error. Therefore, the loss of capacity is quantified only by the antenna error of the signal of interest. This quantity, *per user*, is

$$
\begin{aligned}
\Delta C_u &\approx \mathbb{E}[\log_2(G_p\mathrm{SINR}^G)-\log_2(G_\epsilon\mathrm{SINR}^G)]\\
&= \mathbb{E}[\log_2(\frac{G_p}{G_\epsilon})].,
\end{aligned} \tag{41}
$$

where SINR^G is the SINR without the antenna gain, G_p is the gain due to perfect alignment (e.g. $G_0^{\mathrm{rx}}G_0^{\mathrm{tx}}=G^2$), and G_ϵ is the gain due to error. For sectored antennas, G_ϵ is a binomial random variable which can be fully described by the probability that $G^{\mathrm{tx/rx}}=G$ under error variance of σ^2 (e.g. success probability). We denote this as $p_G(\sigma)$. We omit this derivation for space, but it can be found in [70].

Lemma 3. *The loss in ergodic capacity per user in a mmWave ad hoc network due to beam alignment error with sectored antennas can be approximated as*

$$
\Delta C_u \approx \log_2(G/g)2p_G(\sigma)\left(1-p_G(\sigma)\right)+\log_2(G^2/g^2)\left(1-p_G(\sigma)\right)^2. \tag{42}
$$

We also omit the derivation of the PDF of G_ϵ for Gaussian antennas. In [70], we define K as the fraction of the perfect gain G^2 such that $G_\epsilon = KG^2$. The PDF of K is given as

$$
f_K(z) = \frac{z^{\frac{1}{2\eta\sigma^2}-1}}{2\eta\sigma^2\mathrm{Erf}\left(\frac{\pi}{\sqrt{2}\sigma}\right)^2} \quad z\in[G_{min}^2,1], \tag{43}
$$

where

$$
G_{min} = e^{-\eta\pi^2}. \tag{44}
$$

We evaluate the PDF in (41) to yield our final result.

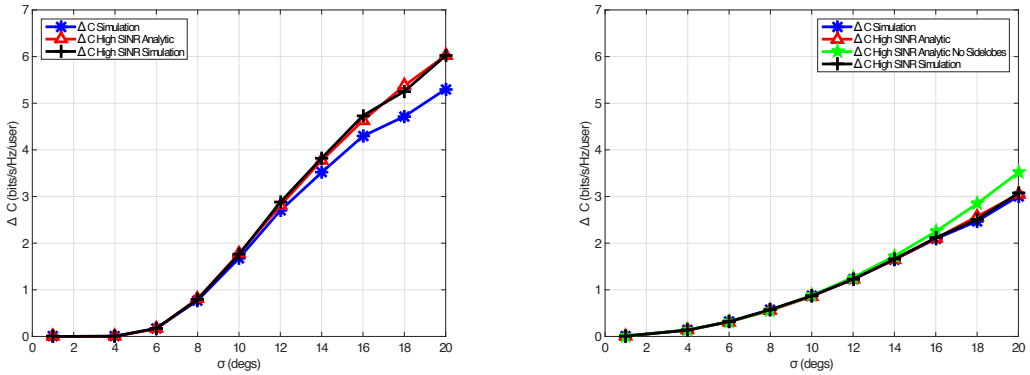

(a) (b)

Fig. 7: The impact of antenna alignment depends on the antenna model used. A $3dB$ beamwidth of 15° is considered. Lemma 4 (green star) closely matches simulation results.

Lemma 4. *The loss in ergodic capacity per user in a mmWave ad hoc network due to beam alignment error with Gaussian antennas can be approximated as*

$$\Delta C_u \approx \frac{4\eta\sigma^2 - 2e^{-\pi^2/\sigma^2}\left(2\eta\sigma^2 + 2\eta\pi^2\right)}{\mathrm{Erf}\left(\frac{\pi}{\sqrt{2}\sigma}\right)^2 \log(4)}. \tag{45}$$

In Fig. 7, we show the differences between Lemma 3 and Lemma 4 (both plots are on the same scale). For both plots in Fig. 7, a beamwidth of 30° is used. The user density is $\lambda = 10^{-5}$. In Fig. 7a, we see that the for $\sigma = 10$ the sectored antenna model yields a 2 bit/sec/Hz/user loss in capacity, but the Gaussian antenna will only lose 1 bit/sec/Hz/user which indicates the need for accurate antenna models. For a user density of $\lambda = 10^{-5}$, the ergodic capacity per user is roughly 8.5 bits/sec/Hz/user; the antenna error at $\sigma = 10$ is about a 12.5% loss. While the Gaussian antenna is still only a model, we believe that it is much closer to the beam pattern of a uniform linear or planar array.

D. Intuition Obtained

Our results indicate that LOS communication leads to much more efficient networks. This motivates the possibility of utilizing relays to *hop* around signal blockage. Relays were studied extensively in the past for lower frequency networks. This problem is worth revisiting in a mmWave environment because of the path-loss gap between LOS and NLOS communication *and* the directionality of antenna array. We also believe that extremely narrow beams degrade the network because of the inevitable antenna alignment error. For example, η scales as $1/\theta_{3dB}^2$ which causes the loss in (45) to increase as the beamwidth decreases.

III. Capacity of Clustered mmWave Mobile Ad Hoc Networks

The ergodic capacity quantifies the average rate that is achievable by *all* the users in the network. The ergodic capacity, also called the area spectral efficiency, has been explored via stochastic geometry in several papers [43] and references therein. MmWave ad hoc networks have been studied in the past as well. We investigated the performance and interference characteristics of homogeneous ad hoc networks [66]–[68]. The performance of body area networks

for wearables was investigated in [77]. Prior work in [66]–[68] considered only the coverage of homogeneous networks, while the work in [77] considers finite network such as a train car for wearables.

Because ad hoc networks are typically limited by nearby interference, accurately modeling the spatial characteristics of the transmitters is needed. In the case of military squads or consumer cliques, users may be clustered together either around a squad leader or a WiFi hotspot, for example. We propose to investigate clustered mmWave ad hoc networks as well as uniform networks. Our previous work showed that mmWave ad hoc networks are line-of-sight (LOS) interference limited [66]; because of this, we are motivated to analyze the ergodic capacity of mmWave LOS clustered and uniform networks, which has not been investigated previously in the literature. Prior work has considered clustered lower frequency ad hoc networks [24], [46]. In [24], the interference properties and coverage of a clustered Neyman-Scott process was derived. The authors presented results for spread-spectrum communication in order to deal with the intra-cluster interference. The performance of clustered interference alignment (IA) networks was developed in [46]. The authors showed that IA can effectively deal with intra-cluster interference for certain cluster sizes as IA outperformed TDMA for larger cluster sizes. In [43], the capacity scaling of ad hoc networks with many receive antennas is quantified, but assumed lower frequency communication.

A. Uniform and Clustered Networks

This work analyzes two different network topologies for user locations: *uniform* and *clustered*. These two topologies exhibit vastly different spatial characteristic as shown in Fig. 2. We consider the standard homogeneous Poisson point process (PPP) [8], [10], [67]. We denote the collection of transmitter locations on $\mathbb{R}^2$ formed by the PPP Φ as the *uniform* network. We denote the intensity of Φ as $\lambda_{\mathrm{u}} = p_{\mathrm{tx}}\lambda$ where p_{tx} is the transmission probability and λ is the intensity of all potential transmitters. Practically speaking, given a finite area of $\mathbb{R}^2$, the transmitters will be randomly uniformly placed within the area. While the homogeneous PPP is attractive to study for its analytic tractability, often it is not representative of realistic user locations. To remedy this limitation, we also use a general Poisson cluster point process Φ_{c}. The cluster process is formed by randomly placing c transmitters in a ball of radius R_c centered at the points of a parent (not necessarily homogeneous) Poisson point process Φ_{p}. Specifically,

$$\Phi_{\mathrm{c}} = \bigcup_{y \in \Phi_{\mathrm{p}}} N^y, \tag{46}$$

where each $N^y \in \mathcal{B}(y, R_c)$ is a finite point process of c points centered on y. Our previous work [68] showed that mmWave networks are LOS-interference limited; we ignore the contribution of NLOS clusters. For simplicity, we assume all users in a cluster N^y are LOS. We call the cluster density λ_{p}. Without loss of generality, due to Slivnyak's theorem, we consider a typical cluster located at the origin N^o by conditioning on the event that a point at the origin exists in Φ_{p}. The cluster process Φ_{c}, therefore, represents the clustered LOS transmitters seen from the typical cluster at the origin. Each transmitter has a receiver located at a fixed distance r_o away with the orientation distributed uniformly in $[0, 2\pi]$ [10]; these receiver points are not part of Φ_{p} nor Φ_{c}. Fig. 2 shows an example realization of the network PPP with the associated receivers.

We consider two MAC protocols in this work: uncoordinated channel access (UCA) and TDMA. For the uniform network under UCA, all the transmitters access the channel within each channel time slot. For the clustered network under UCA, all c transmitters in a cluster access

the channel with each time slot. In TDMA, only one transmitter from each cluster accesses the channel with each time slot. We do not consider TDMA for the uniform network; because we consider single-hop networks, each transmitter-receiver pair is geographically isolated with no coordination between transmitters. In other stochastic geometry work, UCA is considered as ALOHA, but the randomness of the ALOHA channel access would make the number of active transmitters per cluster random; this added randomness reduces the tractability of the analysis. TDMA is widely used in mmWave standards such as 802.11ad [4].

We use the standard unbounded path loss model as

$$\ell(x) = \frac{1}{|x|^{\alpha_{\mathrm{m}}}} \tag{47}$$

where α_{m} is the path loss exponent (PLE). Throughout this paper, we consider only LOS signals (both desired signals and interference signals); as such, α_{m} is typically between 2 and 2.5. Measurements show a lower PLE for line-of-sight (LOS) versus non-line-of-sight (NLOS) signals [55]. This discrepancy is largely caused by building blockage. We use a distance-dependent LOS blockage function $p(r)$. In general, our work is agnostic to the choice of a proper p; we, however, model the blockage as in [12], [13], [66]. As shown in [13] using random shape theory, the probability a link is LOS is given by $p(r) = \exp(-\beta r)$ where β is a function of the average building perimeter and area.

We assume the transmitter and receiver are able to beam steer towards the desired angle of departure and arrival. We model the antenna array with a sectored antenna model

$$G^{\mathrm{tx/rx}} = \begin{cases} N & \theta \in [-\theta_{3dB}, \theta_{3dB}] \\ \frac{1}{N} & \text{otherwise} \end{cases}, \tag{48}$$

where N is the number of antennas at each transmitter and receiver and the mainlobe beamwidth is $2\theta_{3dB}$. The $3dB$ beamwidth of a ULA can be shown to be approximately $\frac{\delta'}{2N}$ where $\delta' = \frac{102\pi}{180}$. The mainlobe of the sectored antenna is then $\frac{\delta'}{N}$. The resultant *system* gain $G^{\mathrm{rx}}G^{\mathrm{tx}}$ is modeled as a discrete random variable κ as in (4). In our previous work, we used the sectored antenna model [12], [66], [68]. When beamforming with the sectored antenna, the channel power is $h = N^2|\gamma|^2$ where $|\gamma|^2$ corresponds to Gamma fading with mean 1 and parameters $(N_{\mathrm{h}}, \frac{1}{N_{\mathrm{h}}})$. For $N_{\mathrm{h}} = 1$, this corresponds to Rayleigh fading, while as $N_{\mathrm{h}} \to \infty$ the fading becomes deterministic. We use a gamma random power term for each signal to capture both the minimal small-scale fading and any other random attenuation effects. At mmWave frequencies, small-scale fading is not a strong phenomenon as shown in [12], [57]. Additionally, it is unlikely the power transfer of the channel is perfect. For example, the scattering and reflection of the mmWave may not transfer 100% of the power; in [59], this is modeled as a exponential random variable.

The received signal of interest for both uniform and clustered networks is

$$y_o = \sqrt{\ell(r_o)h_o\kappa_o A_{\mathrm{m}}}s_o + \sum_{i\in\Phi_{\mathrm{c}}} \sqrt{\ell(x_i - r_o)h_i\kappa_i A_{\mathrm{m}}}s_i + v, \tag{49}$$

where $s_o, s_i \sim \mathcal{N}_{\mathrm{C}}(0, P_t)$, P_t is the signal power, $v \sim \mathcal{N}_{\mathrm{C}}(0, N_o^{\mathrm{m}})$, N_o^{m} is the noise power, $h_o, h_i \sim \Gamma(N_{\mathrm{h}}, \frac{1}{N_{\mathrm{h}}})$, A_{m} is the path loss intercept, and x_i is the random location of each point of point process to the typical receiver. Ignoring misalignment, we assume that the desired signal performs perfect beamforming such that $\kappa_o = N^2$. The received SINR of the uniform/clustered

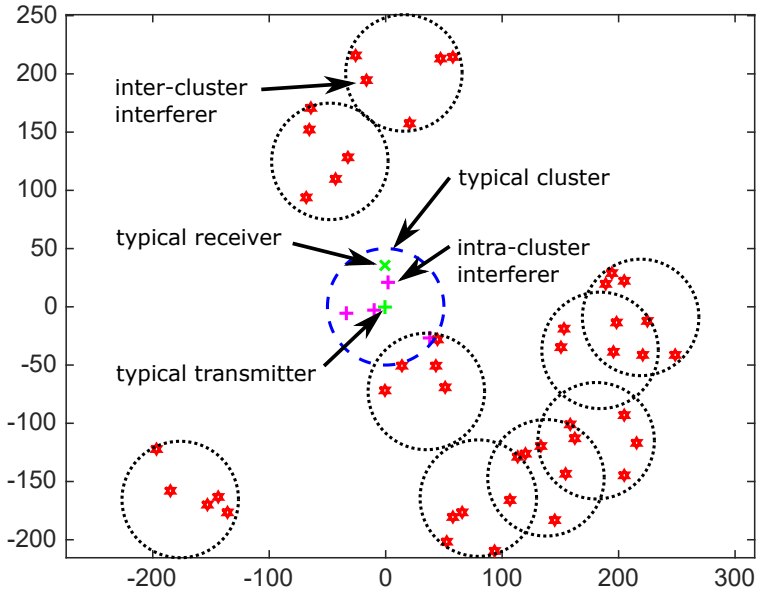

(a)

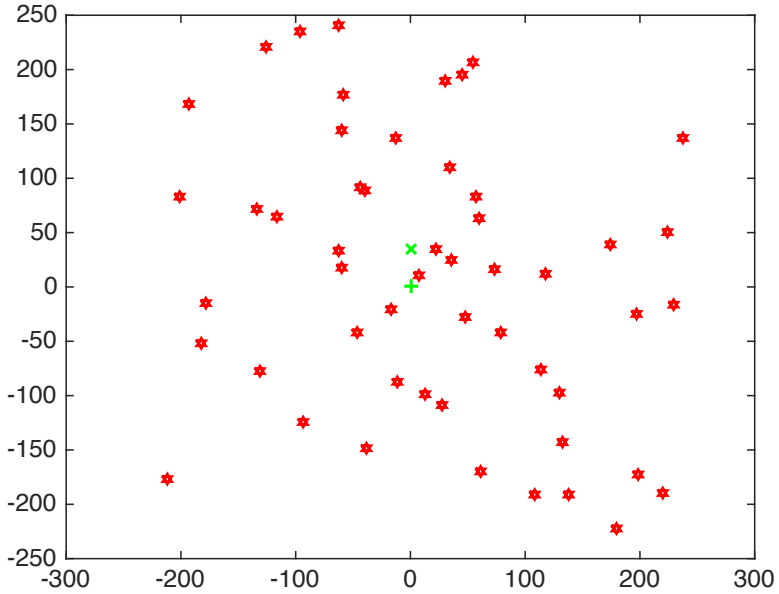

(b)

Fig. 8: An example realization of the LOS clustered network (a) compared to LOS PPP (b). The interfering clusters shown are all LOS from the perspective of the typical cluster at the origin. The dashed blue circle is the boundary for the typical cluster while the black dotted circle is the boundary for the other clusters. The clustered point process exhibits much different spatial properties than the LOS PPP.

networks is

$$\mathrm{SINR}_{\mathrm{u/a}} = \frac{P_t A_{\mathrm{m}} N^2 \ell(r_o) h_o}{N_o^{\mathrm{m}} + \sum_{i \in \Phi/\Phi_{\mathrm{c}}} P_t A_{\mathrm{m}} \ell(x_i - r_o) h_i \kappa_i}, \tag{50}$$

where the interference is either from Φ or Φ_{c}. We note that the signal terms are identical between the two networks which is to be expected. Each network models the signal as an user pair transmitting and receiving at a fixed distance.

B. Key Results: Ergodic Capacity of Clustered mmWave Networks

We are interested in analyzing the ergodic capacity which is the expected sum rate of the network, expressed in terms of $b/s/Hz$. We define this as

$$C^{\Sigma} = \mathbb{E}_{\mathcal{P},h,\kappa} \left[\sum_{i \in \mathcal{P}} \log_2 \left(1 + \mathrm{SINR}_i\right) \right], \tag{51}$$

for some point process of transmitters $\mathcal{P}$. The ergodic capacity as defined in (51) captures the dynamics of the channel and network. As nearby users begin or cease transmitting, the SINR varies over time slots. The fixed-rate approach of our previous work and others does not consider rate-adaption techniques to take advantage of different fading and point process realizations [43], [66]. For the network topologies considered in this paper, we leverage the properties of point processes to simplify (51). In the case of the uniform network with a homogeneous PPP, we can use Slivynak's Theorem such that

$$C_{\mathrm{u}}^{\Sigma} = \lambda_{\mathrm{u}} |A| \mathbb{E}_{\Phi,h,\kappa} \left[\log_2 \left(1 + \mathrm{SINR}_{\mathrm{u}}\right) \right], \tag{52}$$

where A is the area of interest for the network [43] Each transmitter/receiver pair experiences the same SINR on average as the typical pair at the origin [10]. Similarly, we can simplify the clustered network metric to

$$C_{\mathrm{c}}^{\Sigma} = \lambda_{\mathrm{p}} c |A| \mathbb{E}_{\Phi_{\mathrm{c}},h,\kappa} \left[\log_2 \left(1 + \mathrm{SINR}_{\mathrm{a}}\right) \right], \tag{53}$$

where all clusters in the network experience the same signal to interference and noise ratio (SINR) statistics as the *typical* cluster located at the origin [24]. The sum capacity, therefore, is the expected capacity at the origin multiplied by the cluster density c. We present results in terms of the sum ergodic capacity (e.g. $C_{\mathrm{u/e}}^{\Sigma}$) as well as the ergodic capacity of each user $(b/s/Hz/user)$. These quanties are defined as $C_{\mathrm{u}} = \frac{C_{\mathrm{u}}^{\Sigma}}{\lambda_{\mathrm{u}}|A|}$ and $C_{\mathrm{c}} = \frac{C_{\mathrm{c}}^{\Sigma}}{\lambda_{\mathrm{p}} c |A|}$.

Theorem 4. *The ergodic capacity per unit area $(b/s/Hz/user)$ of an uniform outdoor mmWave network is*

$$C_{\mathrm{u}} = \frac{1}{\log(2)} \int_0^{\infty} \frac{e^{-z\theta}}{z} \left[1 - \left(1 + \frac{z \ell(r_o)}{N_h} \right)^{-N_h} \right] \mathcal{L}_{\mathrm{p}}(z) dz \tag{54}$$

with

$$\theta = \frac{N_o^{\mathrm{m}}}{N^2 P_t A_{\mathrm{m}}} \tag{55}$$

and

$$\mathcal{L}_{\mathrm{p}}(z)=\exp\left(-2\pi\lambda_{\mathrm{u}}\sum_{n}p_{n}\int_{0}^{\infty}\left[1-\left(1+\frac{z\ell(r)\kappa_{n}'}{N_{h}}\right)^{-N_{h}}\right]p(r)dr\right). \tag{56}$$

Proof. See [72]. □

The following theorem characterizes the clustered network.

Theorem 5. *The ergodic capacity per user $(b/s/Hz/user)$ of an outdoor clustered mmWave network with directional antennas and uncoordinated channel access is*

$$C_{\mathrm{c}}^{\mathrm{UCA}}=\frac{1}{\log(2)}\int_{o}^{\infty}\frac{e^{-z\theta}}{z}\left[1-\left(1+\frac{z\ell(r_{o})}{N_{h}}\right)^{-N_{h}}\right]\mathcal{L}_{\mathrm{a}}(z)\mathcal{L}_{\mathrm{e}}(z)dz \tag{57}$$

with

$$\theta=\frac{N_{o}^{\mathrm{m}}}{N^{2}P_{t}A_{\mathrm{m}}}, \tag{58}$$

$$\mathcal{L}_{\mathrm{a}}(z)=\left(g(r_{o},z)\right)^{c-1}, \tag{59}$$

$$\mathcal{L}_{\mathrm{e}}(z)=\exp\left(-2\pi\lambda_{\mathrm{p}}\int_{o}^{\infty}\left(1-g(r,z)^{c}\right)rp(r)dr\right), \tag{60}$$

and

$$g(r,z)=\sum_{n}\frac{p_{n}}{\pi R_{c}^{2}}\int_{\mathcal{B}(0,R_{c})}\left(1+\frac{z\ell\left(u-r\right)\kappa_{n}'}{N_{h}}\right)^{-N_{h}}du. \tag{61}$$

Proof. The first term of (57) is a direct application of Lemma 2. The second term is obtained after taking the MGF of the signal fading. The Laplace transform of the intra-cluster interference is given as

$$\begin{aligned}
\mathcal{L}_{\mathrm{a}}(z)&=\mathbb{E}\left[e^{-zI_{\mathrm{a}}}\right] && (62)\\
&=\mathbb{E}\left[e^{-z\sum_{i\in N^{o}}\ell(x_{i}-r_{o})h_{i}\kappa_{i}'}\right] && (63)\\
&\overset{(a)}{=}\mathbb{E}\left[\prod_{i\in N^{o}}\left(1+\frac{z\ell(x_{i}-r_{o})\kappa_{i}'}{N_{\mathrm{h}}}\right)^{-N_{\mathrm{h}}}\right] && (64)\\
&\overset{(b)}{=}\left(\mathbb{E}\left[\left(1+\frac{z\ell(x-r_{o})\kappa_{i}'}{N_{\mathrm{h}}}\right)^{-N_{\mathrm{h}}}\right]\right)^{c-1} && (65)\\
&=\left(\sum_{n}p_{n}\mathbb{E}_{x}\left[\left(1+\frac{z\ell(x_{i}-r_{o})\kappa_{i}'}{N_{\mathrm{h}}}\right)^{-N_{\mathrm{h}}}\right]\right)^{c-1} && (66)\\
&\overset{(c)}{=}\left(\sum_{n}\frac{p_{n}}{\pi R_{c}^{2}}\int_{\mathcal{B}(0,R_{c})}\left(1+\frac{z\ell(x_{i}-r_{o})\kappa_{i}'}{N_{\mathrm{h}}}\right)^{-N_{\mathrm{h}}}dx\right)^{c-1}, && (67)
\end{aligned}$$

where (a) is the MGF of an exponential random variable, (b) is due to independence and the $c-1$ other transmitters in the cluster, and (c) is a substitution due to the generating functional of a point process [20], [72].

The Laplace transform of the inter-cluster interference is given as

$$\mathcal{L}_{\mathrm{e}}(z) = \mathbb{E}\left[e^{-zI_{\mathrm{e}}}\right] \tag{68}$$

$$= \mathbb{E}\left[e^{-z\sum_{i\in\Phi_{\mathrm{c}}}\ell(x_i-r_o)h_i\kappa_i'}\right] \tag{69}$$

$$= \mathbb{E}\left[\prod_{i\in\Phi_{\mathrm{c}}}\left(1+\frac{z\ell(x_i-r_o)\kappa_i'}{N_{\mathrm{h}}}\right)^{-N_{\mathrm{h}}}\right] \tag{70}$$

$$= \mathbb{E}\left[\prod_{y\in\Phi_{\mathrm{p}}}\prod_{x\in N^y}\left(1+\frac{z\ell(y-x-r_o)\kappa'}{N_{\mathrm{h}}}\right)^{-N_{\mathrm{h}}}\right] \tag{71}$$

$$= \mathbb{E}_{\Phi_{\mathrm{p}}}\left[\prod_{y\in\Phi_{\mathrm{p}}}\mathbb{E}_{N^y}\left[\prod_{x\in N^y}\left(1+\frac{z\ell(y-x-r_o)\kappa'}{N_{\mathrm{h}}}\right)^{-N_{\mathrm{h}}}\right]\right] \tag{72}$$

$$\overset{(a)}{=} \mathcal{G}\left(\left(1+\frac{z\ell(y-x-r_o)\kappa'}{N_{\mathrm{h}}}\right)^{-N_{\mathrm{h}}}\right) \tag{73}$$

$$\overset{(b)}{=} \exp\left(-\lambda_{\mathrm{p}}\int_{\mathbb{R}^2}\left(1-g\left(y,z\right)^c\right)p\left(y\right)dy\right) \tag{74}$$

$$\overset{(c)}{=} \exp\left(-2\pi\lambda_{\mathrm{p}}\int_o^\infty\left(1-g\left(r,z\right)^c\right)rp\left(r\right)dr\right), \tag{75}$$

where (a) is due to the definition of a generating functional for a point process [20], [72], (b) is due to the generating functional of the parent process [20], [72] and the stationarity of the inter-cluster interference with respect to r_o, and (c) due to the isometric properties of the inter-cluster interference.

□

Remark: We note the inclusion of $g(r,z)$ (i.e. averaging of the interference signal over the clusters) in (67) and (75) which is typical of clustered point process [24], [46]. Essentially, (67) averages over the typical cluster which is offset by r_o whereas (75) averages over the interference clusters which are offset by r. While a closed form expression, Theorem 5 requires several numerical integrations which can take some time. In particular, the integral over the ball in $g(r,z)$ cannot be reduced by converting to polar coordinates because of the offset of r. It is possible, however, to view the integral as the expectation of the random distance from a given point r to a random point in the ball $\mathcal{B}(0,R_c)$. The distribution of this random distance can be derived to simplify $g(r,z)$ to a single integration.

Specializing the previous theorem to the case where no intra-cluster interference occurs yields the result for TDMA access.

Corollary 1. *The ergodic capacity per user ($b/s/Hz/user$) of an outdoor clustered mmWave*

network with directional antennas and TDMA channel access is

$$C_{\mathrm{c}}^{\mathrm{TDMA}} = \frac{1}{\log(2)} \int_o^{\infty} \frac{e^{-z\theta}}{z} \left[1 - \left(1 + \frac{z\ell(r_o)}{N_h} \right)^{-N_h} \right] \mathcal{L}_{\mathrm{e}}(z) dz \tag{76}$$

with

$$\theta = \frac{N_o^{\mathrm{m}}}{N^2 P_t A_{\mathrm{m}}} \tag{77}$$

and

$$\mathcal{L}_{\mathrm{e}}(z) = \exp\left(-2\pi\lambda_{\mathrm{p}} \int_o^{\infty} \left(1 - g(r,z)\right) r p(r) dr \right). \tag{78}$$

Proof. This is a simplification of Theorem 5 noting that there is no intra-cluster interference and only one interfering transmitter per cluster. □

C. Key Results: Scaling of mmWave Ad Hoc Networks

In this section, the scaling properties of uniform mmWave ad hoc networks as $\lambda_{\mathrm{u}} \to \infty$ are derived. Specifically, we are interested in how the antenna array must grow to accommodate new users (i.e. as λ_{u} grows) with the goal of keeping the *per user* ergodic capacity constant. Because λ_{u} grows large, we switch our focus to the $\mathrm{SIR}_{\mathrm{u}}$.

Theorem 6. *Assume the number of antennas at each user N scales such that $N^2 = t\lambda_{\mathrm{u}}$ for $\alpha_{\mathrm{m}} \in (2, 4]$. Then the capacity scales such that*

$$\frac{C_{\mathrm{u}}^{\Sigma}}{\lambda_{\mathrm{u}}} = \Theta\left(\log_2(1 + t^{\frac{-\alpha_{\mathrm{m}}}{2}}) \right) \tag{79}$$

as $\lambda_{\mathrm{u}} \to \infty$.

Proof. See [69], [72]. □

Remark: Somewhat surprisingly for $\alpha_{\mathrm{m}} \in (2, 4]$, the number of antennas scales independently of the PLE and simply scales with $\Theta(\sqrt{\lambda_{\mathrm{u}}})$. This follows other scaling laws for ad hoc networks [30], [43]. In previous scaling results, the authors showed that the link distance r_o must scale with $\Theta(\sqrt{\lambda_{\mathrm{u}}})$ to match the the interference scaling. Our result shows that the same scaling can be achieved by increasing the antenna array. It is important to note that the upper bound arises from only a single interferer. As the network becomes dense, the closest transmitter to the receiver that is accidentally aligned in the antenna beam pattern essentially limits the overall performance of the system.

D. Intuition Obtained

The results indicate that mmWave ad hoc networks are interference limited for moderately dense deployments of transmitters. The results show that clustered ad hoc networks effectively deal with interference by using directional antennas. In previous lower frequency analysis without directional antennas, intra-cluster interference limited performance severely, but mmWave ad hoc networks can deal with the intra-cluster interference due to the directional antennas. Our results also indicate that antenna arrays can scale sub-linearly with transmitter density to retain the same per-user performance as density increases.

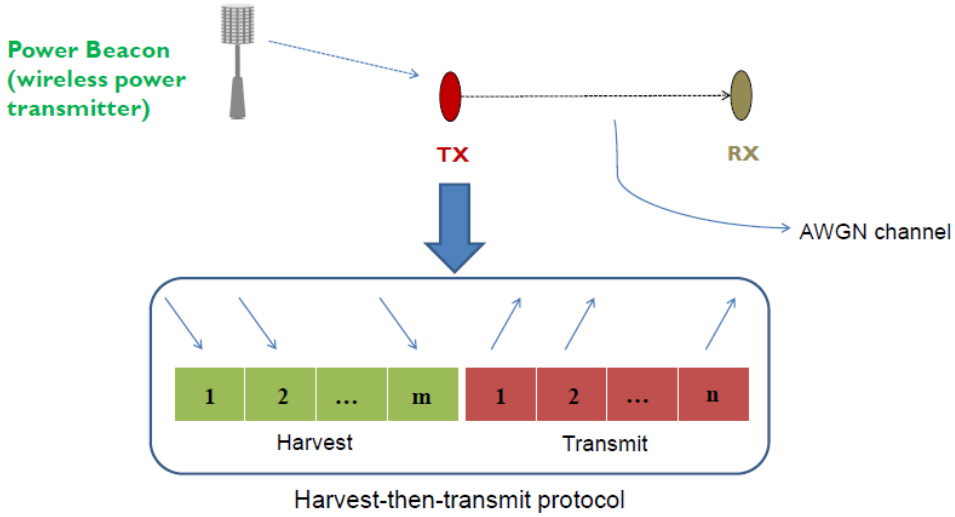

Fig. 9: A power beacon uses wireless energy transfer to charge a sensor (TX), which then uses the harvested energy to communicate with its receiver (RX). A harvest-then-transmit protocol is assumed at the TX, where the first m channel uses are reserved for harvesting and the remaining n channel uses are used for data transmission.

IV. Energy Harvesting for Ad Hoc Networks

Because a wirelessly powered communication system will typically use short packets, the capacity analyses conducted in the asymptotic blocklength regime are not applicable. This has spurred research characterizing the performance of an energy harvesting communication system in the non-asymptotic or finite blocklength regime [23], [27], [45], [81]. Leveraging the finite-length information theoretic framework proposed in [48], [81] characterized the achievable rate for a noiseless binary communications channel with an energy harvesting transmitter. This work was extended to the case of additive white Gaussian noise (AWGN) channel and more general discrete memoryless channels in [23]. For an energy harvesting transmitter operating under a save-then-transmit protocol [47], the achievable rate at the receiver was characterized in the finite blocklength regime [23]. The authors in [27] investigated the mean delay of an energy harvesting channel in the finite blocklength regime. Unlike the work in [23], [27], [81] which assume an infinite battery at the energy harvester, [45] conducted a finite-blocklength analysis for the case of a battery-less energy harvesting channel. Our work differs from prior work on several accounts. The prior work [23], [27], [45], [81] treating short packets falls short of characterizing the performance for the case of wireless energy harvesting. Moreover, most prior work [23], [27], [45], [47], [81] implicitly assumes concurrent harvest and transmit operation, which may be infeasible in practice.

A. MmWave Energy Harvesting Network

We consider a wireless-powered communication system where a wireless power beacon (PB) charges an energy harvesting (EH) device, which then attempts to communicate with another receiver (RX) using the harvested energy. All the nodes are equipped with a single antenna each. We assume that the energy harvester uses a *save-then-transmit* protocol [47] to enable wireless-powered communications. The considered protocol divides the communication frame

consisting of s channel uses (or slots) into an energy harvesting phase having m channel uses, and an information transmission phase having n channel uses. The first m channel uses are used for harvesting energy from the RF signals transmitted by the power beacon, which is then saved in a (sufficiently large) energy buffer. This is followed by an information transmission phase consisting of n channel uses, where the transmitter uses the harvested energy to transmit information to the receiver. We call m the *harvest* blocklength, n the *transmit* blocklength, and $s = m + n$ the *total* blocklength or frame size. We will conduct the subsequent analysis for the non-asymptotic blocklength regime, i.e., for the practical case of *short packets* where the overall blocklength is finite.

The signal transmitted by a power beacon experiences distance-dependent path loss and channel fading before reaching the energy harvesting node. The harvested energy is, therefore, a random quantity due to the underlying randomness of the wireless link. We let random variable $Z_i = \eta\beta P_{\rm PB} H_i$ model the energy harvested in slot i ($i = 1, \cdots, m$), where $\eta \in (0, 1)$ denotes the harvester efficiency, $P_{\rm PB}$ is the PB transmit power, β gives the average large-scale channel gain, while the random variable H_i denotes the small-scale channel gain. Note that we have ignored the energy due to noise since it is negligibly small. We consider quasi-static block flat Rayleigh fading for the PB-EH links such that the channel remains constant over a block, and randomly changes to a new value for the next block. In other words, the energy arrivals within a harvesting phase are fully correlated, i.e., $Z_i = Z_1 \equiv Z, \forall\, i = 1, 2, \cdots, m$, where Z_i is exponentially distributed with mean $\mathbb{E}[Z_i] \triangleq P_E = \eta\beta P_{\rm PB}$. This is motivated by the observation that the harvest blocklength in a *short-packet* communications system would typically be smaller than the channel coherence time.

The energy harvesting phase is followed by an information transmission phase where the EH node attempts to communicate with a destination RX node over an unreliable AWGN channel. We assume that the EH node uses a Gaussian codebook for signal transmission. We let X_ℓ be the signal intended for transmission in slot ℓ with average power $P_{\rm t}$, where $\ell = 1, \cdots, n$, and n is fixed. The resulting (intended) sequence $X^n = (X_1, \cdots, X_n)$ consists of independent and identically distributed (IID) Gaussian random variables such that $X_\ell \sim \mathcal{N}(0, P_{\rm t})$. To transmit the intended sequence X^n over the transmit blocklength, the EH node needs to satisfy the following energy constraints.

$$\sum_{\ell=1}^{k} X_\ell^2 \leq \sum_{i=1}^{m} Z_i \qquad k = 1, 2, \cdots, n \tag{80}$$

The constraints in (80) simplify to $\sum_{\ell=1}^{n} X_\ell^2 \leq mZ$ for the case of correlated energy arrivals. We let $\tilde{X}^n = \left(\tilde{X}_1, \cdots, \tilde{X}_n\right)$ be the transmitted sequence. Note that $\tilde{X}^n \neq X^n$ when the energy constraints are violated as the EH node lacks sufficient energy to put the intended symbols on the channel. The signal received at the destination node in slot ℓ is given by $Y_\ell = \tilde{X}_\ell + V_\ell$, where $V^n = (V_1, \cdots, V_n)$ is an IID sequence modeling the receiver noise such that $V_\ell \sim \mathcal{N}(0, \sigma^2)$ is a zero-mean Gaussian random variable with variance σ^2. Note that any deterministic channel attenuation for the EH-RX link can be equivalently tackled by scaling the noise variance. Similarly, we define $Y^n = (Y_1, \cdots, Y_n)$ as the received sequence.

We now describe the information theoretic preliminaries for the EH-RX link. Let us assume that the EH node transmits a message $W \in \mathcal{W}$ over n channel uses. Assuming W is drawn uniformly from $\mathcal{W} \triangleq \{1, 2, \cdots, M\}$, we define an (n, M)-code having the following features: It uses a set of encoding functions $\{\mathcal{F}_\ell\}_{\ell=1}^{n}$ for encoding the source message $W \in \mathcal{W}$ given the

energy harvesting constraints, i.e., the source node uses $\mathcal{F}_\ell : \mathcal{W} \times \mathbb{R}_+^\ell \to \mathbb{R}$ for transmission slot ℓ, where $\mathcal{F}_\ell(W, Z^\ell) = \tilde{X}_\ell$ given $Z^\ell = (Z_1, \cdots, Z_\ell)$ such that the energy harvesting constraint in (80) is satisfied. Specifically, $\tilde{X}_\ell = X_\ell$ where $X_\ell \sim \mathcal{N}(0, P_{\text{t}})$ is drawn IID from a Gaussian codebook when (80) is satisfied, and $\tilde{X}_\ell = 0$ otherwise. It uses a decoding function $\mathcal{G} : \mathbb{R}^n \to \mathcal{W}$ that produces the output $\mathcal{G}(Y^n) = \hat{W}$, where $Y^n = (Y_1, \cdots, Y_n)$ is the sequence received at the destination node.

We let $\epsilon \in [0, 1)$ denote the target error probability for the noisy communication link. For $\epsilon \in [0, 1)$, an (n, M, ϵ)-code for an AWGN EH channel is defined as the (n, M)-code for an AWGN channel such that the average probability of decoding error $\Pr\{\hat{W} \neq W\}$ does not exceed ϵ. A rate R is *ϵ-achievable* for an AWGN EH channel if there exists a sequence of (n, M_n, ϵ_n)-codes such that $\liminf_{n\to\infty} \frac{1}{n} \log(M_n) \geq R$ and $\limsup_{n\to\infty} \epsilon_n \leq \epsilon$. The *$\epsilon$-capacity* C_ϵ for an AWGN EH channel is defined as $C_\epsilon = \sup\{R : R \text{ is } \epsilon\text{-achievable}\}$.

We now introduce the metrics used for characterizing the performance of the considered *short-packet* wireless-powered communications system. Note that the overall performance is marred by two key events. First, due to lack of sufficient energy, the EH node may not be able to transmit the intended codewords during the information transmission phase, possibly causing a decoding error at the receiver. Second, due to a noisy EH-RX channel, the received signal may not be correctly decoded. For the former, we define a metric called the *energy supply probability*, namely, the probability $\Pr\left[\sum_{i=1}^n X_i^2 \leq mZ\right]$ that an EH node can support the intended transmission. For the latter, we define and characterize the *ϵ-achievable rate* in the finite blocklength regime.

B. Summary of the Key Results

Energy Supply Probability

We define the *energy supply probability* $P_{\text{es}}(m, n, a)$ as the probability that an EH node has sufficient energy to transmit the intended codeword, namely,

$$P_{\text{es}}(m, n, a) = \Pr\left[\sum_{i=1}^{n} X_i^2 \leq mZ\right] \tag{81}$$

for a harvest blocklength m, a transmit blocklength n, and a power ratio $a = \frac{P_{\text{t}}}{P_E}$. Similarly, we define $P_{\text{eo}}(m, n, a) = 1 - P_{\text{es}}(m, n, a)$ as the *energy outage probability* at the energy harvesting node. The following proposition characterizes the energy supply probability for the considered system.

Proposition 1. Assuming the intended transmit symbols $\{X_i\}_{i=1}^n$ are drawn IID from $\mathcal{N}(0, P_t)$, the energy sequence $\{Z_i\}_{i=1}^m = Z$ is fully correlated, and Z follows an exponential law with mean P_E, the energy supply probability is given by

$$P_{\text{es}}(m, n, a) = \frac{1}{\left(1 + \frac{2a}{m}\right)^{\frac{n}{2}}} \tag{82}$$

for $m > 2a$ where $a = \frac{P_{\text{t}}}{P_E}$, while m and n denote the blocklengths for the harvest and the transmit phase.

Proof. The proof follows by leveraging the statistical properties of the random variables. Con-

sider

$$P_{\text{es}}\left(m,n,a\right)=\Pr\left[\sum_{i=1}^{n}X_i^2\leq mZ\right]\overset{(a)}{=}\Pr\left[W\leq\frac{mZ}{P_{\text{t}}}\right]$$
$$\overset{(b)}{=}\mathbb{E}_W\left[e^{-\frac{P_{\text{t}}}{P_E m}W}\right]=\frac{1}{\left(1+\frac{2a}{m}\right)^{\frac{n}{2}}} \tag{83}$$

where (a) follows from the substitution $W=\frac{1}{P_{\text{t}}}\sum_{i=1}^{n}X_i^2$ where W is a Chi-squared random variable with n degrees of freedom. (b) is obtained by conditioning on the random variable W, and by further noting that Z is exponentially distributed with mean P_E. Assuming $m>2a$, the last equation follows from the definition of the moment generating function of a Chi-squared random variable. □

While Proposition 1 is valid for $m>2a$, we note that this is the case of practical interest since it is desirable to operate at $a<1$. Further, the expression in (82) makes intuitive sense as the energy outages would increase with the transmit blocklength n for a given m, and decrease with the harvest blocklength m for a given n. Let us fix P_{t} and P_E. For a given m, we may improve the reliability of the EH-RX communication link by increasing the blocklength n, albeit at the expense of the energy supply probability. With a smaller transmit power P_{t}, the energy harvester is less likely to run out of energy during an ongoing transmission. Therefore, when $m+n$ is fixed, we may reduce P_{t} to meet the energy supply constraint, but this would reduce the channel signal-to-noise ratio (SNR). This underlying tension between the energy availability and the communication reliability will be highlighted throughout the rest of this paper. The following discussion relates the transmit power to the harvest and transmit blocklengths, illustrating some of the key tradeoffs.

Remark: The energy supply probability is more sensitive to the length of the transmit phase compared to that of the harvest phase. This observation also manifests itself in terms of the energy requirements at the transmitter. For instance, to maintain an energy supply probability ρ, it follows from (82) that the power ratio satisfy $a\geq\frac{m}{2}\left(\rho^{-\frac{2}{n}}-1\right)$. Note that the power ratio varies only linearly with the harvest blocklength m, but superlinearly with the transmit blocklength n. This further implies that for a fixed n, doubling the harvest blocklength relaxes the transmit power budget by the same amount. That is, the energy harvester can double its transmit power P_{t} (and therefore the channel SNR) without violating the required energy constraints. In contrast, reducing the transmit blocklength for a given m brings about an exponential increase in the transmit power budget at the energy harvester.

The following corollary treats the scaling behavior of the energy supply probability as the blocklength becomes large.

Corollary 2. When the harvest blocklength m scales in proportion to the transmit blocklength n such that $m=cn$ for some constant $c>0$, the energy supply probability $P_{\text{es}}(m,n,a)$ converges to a limit as n becomes asymptotically large. In other words, $\lim_{n\to\infty}P_{\text{es}}(m,n,a)=e^{-\frac{a}{c}}<1$ such that the limit only depends on the power ratio $a>0$ and the proportionality constant $c>0$. Further, under proportional blocklength scaling, this limit also serves as an upper bound on the energy supply probability for finite blocklengths, i.e., $P_{\text{es}}(m,n,a)\leq e^{-\frac{a}{c}}<1$.

The previous corollary also shows that energy outage is a fundamental bottleneck regardless of the blocklength, assuming at best linear scaling.

Achievable Rates with Wireless Powered Communication

Now, using Proposition 1, we characterize the ϵ-achievable rate of the considered wireless-powered communication system in the finite blocklength regime.

Theorem 7. Given a target error probability $\epsilon \in [0, 1)$ for the noisy channel, the ϵ-achievable rate $R_{EH}(\epsilon, m, n, a, \gamma)$ of the considered system with harvest blocklength m, transmit blocklength n, power ratio a (where $2a < m$), and the SNR $\gamma = \frac{P_t}{\sigma^2}$ is given by

$$R_{EH}(\epsilon, m, n, a, \gamma) = \frac{\frac{n\log(1+\gamma)}{2} - \sqrt{\frac{2+\epsilon}{\epsilon}\frac{\gamma}{\gamma+1}n} - (n)^{\frac{1}{4}} - 1}{n+m} \tag{84}$$

for all tuples (m, n) satisfying

$$m \geq \frac{2a}{\exp\left(\frac{2\ln(1+0.5\epsilon)}{\left(\ln\left[\frac{2+\epsilon}{\epsilon^2}\right]\right)^4}\right) - 1} \tag{85}$$

and

$$n \leq 2\frac{\ln(1+0.5\epsilon)}{\ln\left(1+\frac{2a}{m}\right)}. \tag{86}$$

Proof. See [38, Appendix]. □

For a given target error probability ϵ, a harvest blocklength m can support a transmit blocklength only as large as in (86). Moreover, a sufficiently large m, as given in (85), is required for a sufficiently large n to meet the target error probability ϵ. The following proposition provides an analytical expression for the achievable rate in the asymptotic blocklength regime. We note that the asymptotic results provide a useful analytical handle for the non-asymptotic case as well.

Proposition 2. Let $R^{\infty}_{\text{EH}}(\epsilon, a, \gamma)$ denote the asymptotic achievable rate as the transmit blocklength $n \to \infty$, i.e., $R^{\infty}_{\text{EH}}(\epsilon, a, \gamma) = \lim_{n\to\infty} R_{\text{EH}}(\epsilon, m, n, a, \gamma)$. It is given by

$$R^{\infty}_{\text{EH}}(\epsilon, a, \gamma) = L(a, \epsilon)C^{\infty}_{\text{AWGN}}(\gamma) \tag{87}$$

where

$$C^{\infty}_{\text{AWGN}}(\gamma) = \frac{1}{2}\log(1+\gamma), \quad \gamma \geq 0 \tag{88}$$

denotes the capacity of an AWGN channel without the energy harvesting constraints, whereas

$$L(a, \epsilon) = \frac{1}{1 + \frac{a}{\log(1+0.5\epsilon)}}, \quad a \geq 0,\ \epsilon \in [0, 1) \tag{89}$$

where $L(a, \epsilon) \in [0, 1]$ such that $1 - L(a, \epsilon)$ gives the (fractional) loss in capacity due to energy harvesting constraints.

Proof. Using (84), $R_{\text{EH}}^{\infty}(\epsilon, a, \gamma)$ can be expressed as

$$R_{\text{EH}}^{\infty}(\epsilon, a, \gamma) = \lim_{n\to\infty} \frac{\frac{n\log(1+\gamma)}{2} - \sqrt{\frac{2+\epsilon}{\epsilon}\frac{\gamma}{\gamma+1}n} - (n)^{\frac{1}{4}} - 1}{n+m} \tag{90}$$

$$\overset{(a)}{=} \lim_{n\to\infty} \frac{1}{1+\frac{m}{n}} \frac{\log(1+\gamma)}{2} \tag{91}$$

$$\overset{(b)}{=} \lim_{n\to\infty} \frac{1}{1+\frac{2a}{n[1+0.5\epsilon]^{\frac{2}{n}}-1}} \frac{\log(1+\gamma)}{2} \tag{92}$$

$$\overset{(c)}{=} \underbrace{\frac{1}{1+\frac{a}{\log(1+0.5\epsilon)}}}_{L(a,\epsilon)} \underbrace{\frac{\log(1+\gamma)}{2}}_{C_{\text{AWGN}}^{\infty}(\gamma)} \tag{93}$$

where (a) follows since the higher order terms in (84) vanish as $n \to \infty$. Note that for a given ϵ and a, m and n should satisfy (85) and (86). (b) is obtained by substituting $m = \frac{2a}{[1+0.5\epsilon]^{\frac{2}{n}}-1}$ from (86), and by further assuming that $n \geq \left(\log\left(\frac{2+\epsilon}{\epsilon^2}\right)\right)^4$. Finally, (c) follows by noting that $\lim_{n\to\infty} n\left((1+x)^{\frac{2}{n}} - 1\right) = 2\log(1+x)$. □

Remark: Proposition 2 reveals a fundamental communications limit of the considered wireless-powered system. In order to guarantee an ϵ-reliable communication over n channel uses, the node first needs to accumulate sufficient energy during the initial harvesting phase. A sufficiently large m helps improve the energy availability at the transmitter. This harvesting overhead, however, causes a rate loss (versus a non-energy harvesting system) as the first m channel uses are reserved for harvesting. Moreover, as the transmit blocklength n grows, so does the length of the initial harvesting phase m, resulting in an inescapable performance limit on the communication system. This limit depends on i) the power ratio a, and ii) the required reliability ϵ, and is captured by the prelog term $L(a, \epsilon)$ in (89) for a given γ. Moreover, this behavior is more visible for latency-constrained systems where the total blocklength is fixed.

Corollary 3. As the power ratio $a \to 0$ in (87), the asymptotic achievable rate converges to the capacity of a non-energy harvesting AWGN channel, i.e., $\lim_{a\to 0} R_{\text{EH}}^{\infty}(\epsilon, a, \gamma) = C_{\text{AWGN}}^{\infty}(\gamma)$.

For optimal performance, the energy harvesting node needs to use the *right* amount of transmit power. On the one hand, reducing P_{t} helps improve the energy supply probability as a packet transmission is less likely to face an energy outage. On the other hand, it is detrimental for the communication link as it lowers the SNR. We now quantify the optimal transmit power that maximizes the asymptotic achievable rate for a given set of parameters. We note that many of the analytical insights obtained for the asymptotic regime are also useful for the non-asymptotic regime (see Remark 3).

Corollary 4. For a given P_E, there exists an optimal transmit power that maximizes the achievable rate. We let $P_{\text{t},\infty}^{*}$ be the rate-maximizing transmit power in the asymptotic blocklength regime. It follows that $P_{\text{t},\infty}^{*}(\epsilon, P_E, \sigma^2) =$

$$\sigma^2 \left(\frac{\frac{P_E}{\sigma^2}\log(1+0.5\epsilon) - 1}{\text{W}\left[\left(\frac{P_E}{\sigma^2}\log(1+0.5\epsilon) - 1\right)e^{-1}\right]} - 1 \right) \tag{94}$$

where $\text{W}[\cdot]$ is the Lambert W-function.

Plugging $P_{\text{t}} = P_{\text{t},\infty}^{*}$ in Proposition 2 gives the optimal achievable rate in the asymptotic

blocklength regime. Furthermore, when P_{t} is fixed, the achievable rate improves monotonically with P_E due to an increase in the energy supply probability.

C. Intuition Obtained

Our results indicate that the optimal transmit power for the asymptotic case serves as a conservative estimate for the optimal transmit power for the non-asymptotic case. Moreover, the achievable rate in the non-asymptotic regime obtained using the asymptotically optimal transmit power, gives a tight lower bound for the optimal achievable rate in the non-asymptotic regime. This suggests that Corollary 4 provides a useful analytical handle for transmit power selection even for the finite blocklength regime. This is despite the fact that the resulting rate for the non-asymptotic case could be much smaller than that for the asymptotic case.

V. Ergodic Rate and Overhead of Ad Hoc Networks

Because ad hoc networks are typically limited by nearby interference, accurately modeling the spatial characteristics of the transmitters is needed. In the case of military squads or consumer cliques, users may be clustered together either around a squad leader or a WiFi hotspot, for example. We investigate clustered mmWave ad hoc networks as well as uniform networks. Our previous work showed that mmWave ad hoc networks are line-of-sight (LOS) interference limited [66]; because of this, we are motivated to analyze the ergodic rate of mmWave LOS clustered and uniform networks, which has not been investigated previously in the literature. Prior work has considered clustered lower frequency ad hoc networks [24], [46]. We consider the issue of communicating *between* clusters while maintaining adequate data rates *within* clusters. We call this the intra-ϵ inter-cluster coverage.

A key enabling technology for mmWave networks is active steerable beamforming that directs the RF energy towards the intended receiver. By directing the energy, the transmitter and receiver achieve beamforming gain to overcome the increased free space path loss due to the higher frequency of mmWave communication. The communication link is dependent on the beamforming gain to truly take advantage of the mmWave spectrum; additionally, errors in the beamforming can severly impact the efficiency of communication. It is unclear, however, how to best train wireless nodes in a mmWave ad hoc network. Due to latency concerns for the user, overhead in protocol design, and channel conditions changing, the beamforming method should be done quickly. Cellular mmWave training can be accelerated by reducing the number of beam sweeping steps at the cost of gain during the training procedure as shown in [44]. In the cellular case, the user connects to the strongest base station whereas the strongest signal in an ad hoc network may be interference. Because of this, the training sequence for mmWave ad hoc networks must be robust to interference.

A. System Model for MmWave Tactical Ad Hoc Network

This work analyzes two different network topologies for user locations: *uniform* and *clustered*. These two topologies exhibit vastly different spatial characteristic as shown in Fig. 8. We consider the standard homogeneous Poisson point process (PPP) [8], [10], [67]. We denote the collection of transmitter locations on $\mathbb{R}^2$ formed by the PPP Φ as the *uniform* network. We denote the intensity of Φ as $\lambda_{\mathrm{u}} = p_{\mathrm{tx}}\lambda$ where p_{tx} is the transmission probability and λ is the intensity of all potential transmitters. Practically speaking, given a finite area of $\mathbb{R}^2$, the transmitters will be randomly uniformly placed within the area. While the homogeneous PPP is attractive to study

for its analytic tractability, often it is not representative of realistic user locations. To remedy this limitation, we also use a general Poisson cluster point process $\Phi_{\rm c}$. The cluster process is formed by randomly placing c transmitters in a ball of radius R_c centered at the points of a parent (not necessarily homogeneous) Poisson point process $\Phi_{\rm p}$. Specifically,

$$\Phi_{\rm c} = \bigcup_{y \in \Phi_{\rm p}} N^y, \tag{95}$$

where each $N^y \in \mathcal{B}(y, R_c)$ is a finite point process of c points centered on y. Our previous work [68] showed that mmWave networks are LOS-interference limited; we ignore the contribution of NLOS clusters. For simplicity, we assume all users in a cluster N^y are LOS. We call the cluster density $\lambda_{\rm p}$. Without loss of generality, due to Slivnyak's theorem, we consider a typical cluster located at the origin N^o by conditioning on the event that a point at the origin exists in $\Phi_{\rm p}$. The cluster process $\Phi_{\rm c}$, therefore, represents the clustered LOS transmitters seen from the typical cluster at the origin. Each transmitter has a receiver located at a fixed distance r_o away with the orientation distributed uniformly in $[0, 2\pi]$ [10]; these receiver points are not part of $\Phi_{\rm p}$ nor $\Phi_{\rm c}$. Fig. 8 shows an example realization of the network PPP with the associated receivers.

We use the standard unbounded path loss model as

$$\ell(x) = \frac{1}{|x|^{\alpha_{\rm m}}} \tag{96}$$

where $\alpha_{\rm m}$ is the path loss exponent (PLE). Throughout this paper, we consider only LOS signals (both desired signals and interference signals); as such, $\alpha_{\rm m}$ is typically between 2 and 2.5. Measurements show a lower PLE for line-of-sight (LOS) versus non-line-of-sight (NLOS) signals [55]. This discrepancy is largely caused by building blockage. We use a distance-dependent LOS blockage function $p(r)$. In general, our work is agnostic to the choice of a proper p; we, however, model the blockage as in [12], [13], [66]. As shown in [13] using random shape theory, the probability a link is LOS is given by $p(r) = \exp(-\beta r)$ where β is a function of the average building perimeter and area.

We assume the transmitter and receiver are able to beam steer towards the desired angle of departure and arrival (AoD/AoA). We model the antenna array with a sectored antenna model

$$G^{\rm tx/rx} = \begin{cases} N & \theta \in [-\theta_{3dB}, \theta_{3dB}] \\ \frac{1}{N} & \text{otherwise} \end{cases}, \tag{97}$$

where N is the number of antennas at each transmitter and receiver and the mainlobe beamwidth is $2\theta_{3dB}$. The $3dB$ beamwidth of a ULA can be shown to be approximately $\frac{\delta'}{2N}$ where $\delta' = \frac{102\pi}{180}$. The mainlobe of the sectored antenna is then $\frac{\delta'}{N}$. The resultant *system* gain $G^{\rm rx}G^{\rm tx}$ is modeled as a discrete random variable κ such that

$$\kappa = \begin{cases} N^2 & \text{w.p. } p_1 = \frac{\delta^2}{N^2} \\ 1 & \text{w.p. } p_2 = 2\left(1 - \frac{\delta}{N}\right)\frac{\delta}{N} \\ N^{-2} & \text{w.p. } p_3 = \left(1 - \frac{\delta}{N}\right)^2, \end{cases} \tag{98}$$

where $\delta = \frac{\delta'}{2\pi}$. In our previous work, we used the sectored antenna model [12], [66], [68]. When beamforming with the sectored antenna, the channel power is $h = N^2|\gamma|^2$ where $|\gamma|^2$ corresponds to Gamma fading with mean 1 and parameters $(N_{\rm h}, \frac{1}{N_{\rm h}})$. For $N_{\rm h} = 1$, this corresponds to Rayleigh fading, while as $N_{\rm h} \to \infty$ the fading becomes deterministic. We use a gamma random power term

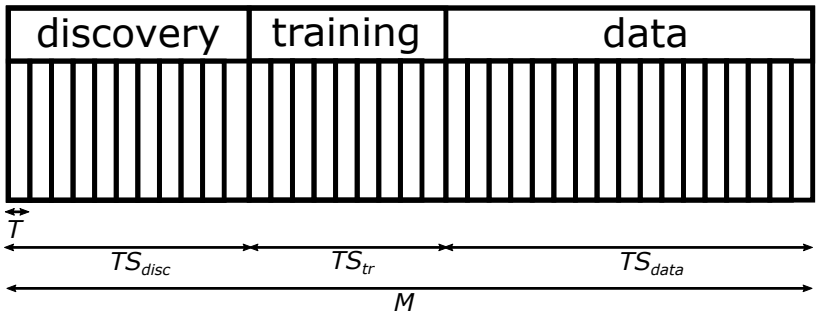

Fig. 10: The time-slotted design of the proposed system. Each transmission opportunity is T sec long. The discovery period lasts for TS_{disc} sec, the training periods lasts for TS_{tr} sec, and the remain transmissions are used for data. The total time is M sec.

for each signal to capture both the minimal small-scale fading and any other random attenuation effects. At mmWave frequencies, small-scale fading is not a strong phenomenon as shown in [12], [57]. Additionally, it is unlikely the power transfer of the channel is perfect. For example, the scattering and reflection of the mmWave may not transfer 100% of the power; in [59], this is modeled as a exponential random variable.

To analyze the effect of beam training overhead, we use a slotted transmission strategy divided into three phases: *discovery*, *training*, and *data*, Fig. 10. During the discovery phase, one user in the dipole pair sends a beacon-like packet. During the training phase, the feedback of best beamforming slot is done. During the data phase, the actual user data is transmitted. For simplicity, we assume the network uses a fixed transmit time T sec for each transmission opportunity. We denote the number of transmission slots for discover, training, and data as S_{disc}, S_{tr}, and S_{data}, respectively. The total time a user spends discovering and training is then $T \cdot (S_{\text{disc}} + S_{\text{tr}})$ sec. We denote the total *transmission interval* which includes the *discovery*, *training*, and *data* slots and lasts for M sec. The system is considered to be invariant to small-scale fading over the T sec. Additionally, the network is assumed to invariant to large-scale fading effects (e.g AoA / AoD / blockage) for M sec.

We use modified methods from [44]: *baseline*, *fast-training*, and *fast-discovery and training*. These methods are variations on the beamsweeping algorithms from standards such as [4]. For all methods, during the discovery phase, one user (e.g. the primary) transmits the beacon-like frames while the other user (e.g. the secondary) listens; during the training phase, the secondary user sends feedback over one or many beams while the primary user listens. In the baseline method, during the discovery phase, each user in the dipole pair sweeps over its beam patterns which takes $S_{\text{disc}} = N^2$ slots. During the training phase, the primary user sweeps over its beams again while the secondary user transmits using the best beam from the discovery phase; this takes $S_{\text{tr}} = N$ slots. In the fast-training method, during the discovery phase, each user in the dipole pair sweeps over its beam patterns which takes $S_{\text{disc}} = N^2$ slots. During the training phase, the primary user listens omni-directionally while the other user fixes its beam on the best result from the discovery phase; this takes $S_{\text{tr}} = 1$ slot. In the fast-discovery and training method, during the discovery phase, the primary user sweeps over its beam patterns while the secondary user listens omni-directionally which takes $S_{\text{disc}} = N$ slots. During the training phase, the roles are swapped; this takes another $S_{\text{tr}} = N$ slots.

B. Key Results: Intra-ϵ Inter-cluster Coverage

We consider two coverage metrics in the clustered case: *intra-cluster* coverage and *inter-cluster* coverage. We say users are covered if $\mathbb{P}[\mathrm{SINR} > \Gamma] \geq 1-\epsilon$. This ensures that users can support a data rate $R = \log_2(1+\Gamma)$ at least $(1-\epsilon)\%$ of the time. We denote the intra and inter-cluster coverage by $\mathrm{P_a}(\Gamma) = \mathbb{P}[\mathrm{SINR_a} > \Gamma]$ and $\mathrm{P_e}(\Gamma) = \mathbb{P}[\mathrm{SINR_e} > \Gamma]$. The intra-cluster coverage is the coverage between a receiver and transmitter operating within the same cluster head. This is useful for peer-to-peer gaming applications or soldiers of the same squad sharing data. The inter-cluster coverage is the coverage between the cluster heads. This characterizes data propagation throughout the network; if clusters are isolated (e.g poor inter-cluster coverage), the data between squads will not propagate.

For inter-cluster communication, we define another SINR as

$$\mathrm{SINR_e} = \frac{P_t A_{\mathrm{m}} N^2 r_{\mathrm{e}}^{-\alpha_{\mathrm{m}}} h_o}{N_o^{\mathrm{m}} + \sum_{i \in \Phi_{\mathrm{c}}} P_t A_{\mathrm{m}} \ell(x_i - r_o) h_i \kappa_i}, \tag{99}$$

where r_{e} is the random distance to the nearest cluster center. For simplicity, we consider this point rather than a point randomly located in the cluster. The distribution of this random distance is $f_{r_{\mathrm{e}}}(r)$ given in [13, Corollary 10.1].

In this section, for clarity and brevity, we consider $N_{\mathrm{h}} = 1$ as it simplifies the expressions. Our previous work considered coverage and transmission rate of mmWave ad hoc networks for $N_{\mathrm{h}} > 1$. To see a derivation with the added complexity, see [66]. We are interested in the balance between the inter and intra cluster coverage. To begin, we define the transmission rate of the intra-cluster communication to be

$$q(\epsilon, \Gamma) = \arg\max_{\lambda_{\mathrm{p}}} \ \text{s.t.} \ \mathrm{P_a}(\Gamma) \geq 1-\epsilon, \tag{100}$$

which is the largest cluster density while maintaining the intra-cluster coverage requirement. Because $\mathrm{P_a}(\Gamma)$ is a decreasing function with λ_{p}, it suffices to solve $\mathrm{P_a}(\Gamma) = 1-\epsilon$ for λ_{p}. Given this cluster density, we can evaluate $\mathrm{P_e}(\Gamma)$. We define a metric to quantify this as the intra-ϵ inter-cluster coverage. Specifically, we define it as

$$P(\epsilon, \Gamma) = \mathbb{P}[\mathrm{SINR_e} > \Gamma | \lambda_{\mathrm{p}} = q(\epsilon, \Gamma)]. \tag{101}$$

This metric quantifies the probability that an inter-cluster link is covered while ensuring that each intra-cluster link is covered at least $(1-\epsilon)\%$ of the time. As the cluster density increases, r_{e} decreases, but the communication within the cluster must deal with more interference.

Corollary 1. *The intra-ϵ inter-cluster coverage of an outdoor clustered mmWave ad hoc network is*

$$P(\epsilon, \Gamma) = \int_o^\infty e^{-r_{\mathrm{e}}^{\alpha_{\mathrm{m}}} \theta \Gamma} \mathcal{L}_{\mathrm{a}}(r_{\mathrm{e}}^{\alpha_{\mathrm{m}}} \Gamma) \mathcal{L}_{\mathrm{e}}(r_{\mathrm{e}}^{\alpha_{\mathrm{m}}} \Gamma) f_{r_{\mathrm{e}}}(r) dr, \tag{102}$$

with

$$\theta = \frac{N_o^{\mathrm{m}}}{N^2 P_t A_{\mathrm{m}}}, \tag{103}$$

$$g(r, z) = \sum_n \frac{p_n}{\pi R_c^2} \int_{\mathcal{B}(0, R_c)} \left(1 + \frac{z\ell\left(u - r\right)\kappa_n'}{N_h}\right)^{-N_h} du. \tag{104}$$

The cluster density $\lambda_{\rm p}$ in $\mathcal{L}_{\rm e}$ is equal to

$$q(\epsilon,\Gamma)=\frac{-\log\left(\frac{1-\epsilon}{\exp(-r_o^{\alpha_{\rm m}}\theta\Gamma)\mathcal{L}_{\rm a}(r_o^{\alpha_{\rm m}}\Gamma)}\right)}{2\pi W(r_o^{\alpha_{\rm m}}\Gamma)}, \tag{105}$$

with

$$W(r_o^{\alpha_{\rm m}}\Gamma)=\int_o^{\infty}\left(1-\left(g(r,r_o^{\alpha_{\rm m}}\Gamma)\right)^c\right)rp\left(r\right)dr. \tag{106}$$

Proof. First, we must evaluate the transmission rate of intra-cluster communication. We compute $\mathrm{P_a}(\Gamma)$ in the standard way by re-arranging the $\mathrm{SINR_a}$ to exploit the exponential fading such that

$$\begin{aligned}\mathbb{P}\left[\mathrm{SINR_a}>\Gamma\right]&=\mathbb{P}\left[h_o>\left(r_o^{\alpha_{\rm m}}\theta+r_o^{\alpha_{\rm m}}I\right)\Gamma\right] &(107)\\ &=\mathbb{E}\left[\exp\left(-r_o^{\alpha_{\rm m}}\theta\Gamma-r_o^{\alpha_{\rm m}}I\Gamma\right)\right] &(108)\\ &=e^{-r_o^{\alpha_{\rm m}}\theta\Gamma}\mathbb{E}\left[\exp\left(-r_o^{\alpha_{\rm m}}\Gamma(I_{\rm a}+I_{\rm e})\right)\right] &(109)\\ &=e^{-r_o^{\alpha_{\rm m}}\theta\Gamma}\mathcal{L}_{\rm a}(r_o^{\alpha_{\rm m}}\Gamma)\mathcal{L}_{\rm e}(r_o^{\alpha_{\rm m}}\Gamma), &(110)\end{aligned}$$

where

$$\theta=\frac{N_o^{\rm m}}{N^2P_tA_{\rm m}}. \tag{111}$$

Because $\lambda_{\rm p}$ only appears in $\mathcal{L}_{\rm e}$ outside the integration, we can invert (110) to obtain the transmission rate as

$$q(\epsilon,\Gamma)=\frac{-\log\left(\frac{1-\epsilon}{\exp(-r_o^{\alpha_{\rm m}}\theta\Gamma)\mathcal{L}_{\rm a}(r_o^{\alpha_{\rm m}}\Gamma)}\right)}{2\pi W(r_o^{\alpha_{\rm m}}\Gamma)}. \tag{112}$$

To evaluate $\mathrm{P_e}(\Gamma)$, we note that it is equivalent to to $\mathrm{P_a}(\Gamma)$, but r_o is replaced with $r_{\rm e}$ and must be integrated over $f_{r_{\rm e}}(r)$.

The Laplace transform of the intra-cluster interference is given in (67).

The Laplace transform of the inter-cluster interference is given in (75). □

Comment: Corollary 1 provides a framework for optimizing the network given a combination network parameters such as cluster density, communication range, and cluster range. By adding clusters to the network, the distance between the clusters shrinks, but the interference within a cluster increases; the framework allows the right balance between intra-cluster and inter-cluster data rate to be achieved. We define Corollary 1 such that the SINR threshold is the same for intra-cluster and inter-cluster communication. Having a different SINR threshold would give different guaranteed rates for intra-cluster versus inter-cluster communication. This could cause data bottlenecks if the goal of the network was to allow data to propogate both within the cluster and between the clusters. While we consider the same rate requirements, Corollary 1 can be modified to allow for different rate requirements (e.g. $\Gamma_{\rm a},\Gamma_{\rm e}$).

C. Key Results: Ergodic Rate with Beamforming Overhead

During the discovery phase, we assume that no central coordinating is available to ensure discovery for each user is done at the same time. Because of this limitation of ad hoc networks, a popular method of cellular mmWave discovery, (near)-orthogonal pilots, cannot be used [7]. If

the other users in the network are transmitting data during the discovery period, the gain of pilots is lost. Instead, ad hoc networks must rely on antenna gain to overcome the interference and path-loss during discovery. The discovery and training phases of the transmission interval are considered successful if the transmission during the desired beam in the discovery and training phases exceeds an SINR threshold. Specifically,

$$P_{\mathrm{disc+tr}} = \mathbb{P}\left[\mathrm{SINR}_{\mathrm{disc}} > \Gamma\right] \mathbb{P}\left[\mathrm{SINR}_{\mathrm{tr}} > \Gamma\right] \tag{113}$$

where $\mathrm{SINR}_{\mathrm{disc}}$ is the SINR during the discovery phase and $\mathrm{SINR}_{\mathrm{tr}}$ is the SINR during the training phase. The variables for $\mathrm{SINR}_{\mathrm{disc}}$ and $\mathrm{SINR}_{\mathrm{disc}}$ are the same as 50, but with the gain values appropriately chosen. In the baseline method, the gain during discovery and training is N^2. In the fast-training method, the gain during discovery is N^2, but the gain during training is N. In the fast-discovery and training method, the gain in both phases is N.

If we treat each discovery and training attempt as a Bernoulli random variable, we can define the PMF of the discrete random variable ν_{disc}, where ν_{disc} is the number of discovery and training phases for both phases to be successful. The number of discovery attempts to successfully join the network, ν_{disc} is modeled as a geometric random variable. The expected time to begin transmission is then [44]

$$\tau = \mathbb{E}[\nu_{\mathrm{disc}}\left(M-1\right)] + TS_{\mathrm{disc}} + TS_{\mathrm{tr}} \tag{114}$$

$$= \frac{M-1}{P_{\mathrm{disc+tr}}} + TS_{\mathrm{disc}} + TS_{\mathrm{tr}}. \tag{115}$$

We omit the details here, but analytic solutions to $P_{\mathrm{disc+tr}}$ are available for various network configurations in our previous work [71], [72].

The effect of overhead on ergodic rate is captured by

$$R = \frac{TS_{\mathrm{disc}} + TS_{\mathrm{tr}}}{M} P_{\mathrm{disc+tr}} \mathbb{E}_{\mathcal{P},h,\kappa}\left[\sum_{i\in\mathcal{P}} \log_2\left(1+\mathrm{SINR}_i\right)\right], \tag{116}$$

where the first term represents the deterministic time the beamforming takes each transmission interval. The second term adjusts the ergodic rate for the expected number of transmission intervals it will take for the training to be successful. The final term is the ergodic rate of the network. Analytic solutions to the ergodic rate are available for both uniform and clustered networks in our previous work [71], [72].

Comment: By finding the minima of (115) and (116), which will be explored in future work, the optimum parameters for training length or user density can be found based on the other network parameters. This will allow the development of optimum training strategies with respect to factors such as user mobility.

D. Intuition Obtained

The results indicate that mmWave ad hoc network clusters can remain connected to each other if the required data rate between clusters is small even for tightly packed clusters. Our results show that beamforming gain at both the receiver and transmitter is required for quick and successful training in mmWave ad hoc networks. This requires exhaustive search which increases as N^2. Without the antenna gain at the receiver and transmitter, the mmWave blockage and interference prohibit successful reception of training frames.

VI. Energy Harvesting for Ad Hoc Networks

Our previous work has shown that wireless energy and/or information transfer could benefit from mmWave technology [34], [37], [78]. In [34], an outdoor urban scenario with mmWave transmitters and harvesters was considered. Using stochastic geometry, the energy coverage probability at an energy harvester was characterized while incorporating blockages due to buildings. This work was extended in [37] to include simultaneous wireless information and energy transfer and the joint energy-and-information coverage probability was characterized. In [78], a mmWave wireless-powered communication system with power transfer in the downlink and information transfer in the uplink was analyzed in terms of the average uplink achievable rate. In [50], a directional ad hoc network with joint information and energy transfer was investigated in the presence of building blockages. While the existing work [34], [37], [50], [78] mainly considers blockage due to buildings, we treat each node as a potential human-body blockage, thus coupling the blockage density with the network density. The performance of mmWave systems with body blockages has chiefly been considered in the context of cellular [25] or indoor wearable communication systems [76]. We provide an analytical treatment of the overall success probability while explicitly taking the network load into account.

Because remotely-powered communications will feature short packets, the capacity analyses conducted in the asymptotic blocklength regime are not applicable. This has spurred research characterizing the performance of an energy harvesting communication system in the non-asymptotic or finite blocklength regime [23], [27], [45], [81]. Leveraging the finite-length information theoretic framework proposed in [48], [81] characterized the achievable rate for a noiseless binary communications channel with an energy harvesting transmitter. This work was extended to the case of additive white Gaussian noise (AWGN) channel and more general discrete memoryless channels in [23]. For an energy harvesting transmitter operating under a save-then-transmit protocol [47], the achievable rate at the receiver was characterized in the finite blocklength regime [23]. The authors in [27] investigated the mean delay of an energy harvesting channel in the finite blocklength regime. Unlike the work in [23], [27], [81] which assume an infinite battery at the energy harvester, [45] conducted a finite-blocklength analysis for the case of a battery-less energy harvesting channel. Our work differs from prior work on several accounts. The prior work [23], [27], [45], [81] treating short packets falls short of characterizing the performance for the case of wireless energy harvesting. Moreover, most prior work [23], [27], [45], [47], [81] implicitly assumes concurrent harvest and transmit operation, which may be infeasible in practice. While the previous work focuses on isolated setups, we leverage a stochastic geometry framework to study a wireless-powered communication network with short packets.

A. Model for Wireless Energy Transfer in MmWave Tactical Networks

We consider a wireless network where node locations follow a homogeneous Poisson point process (PPP) $\Phi(\lambda)$ of density λ. We assume that the network consists of two types of nodes i) power beacons (PBs) and ii) energy harvesters (EHs). This may model a tactical scenario where soldiers equipped with PB devices transfer RF power to those with EH devices. We assume that a fraction $\rho \in (0,1)$ of the deployed nodes serve as PB nodes, while a fraction $1-\rho$ as EH nodes. That is, the PPP $\Phi(\lambda)$ is independently thinned into two independent PPPs $\Phi_{\mathrm{PB}}(\lambda_{\mathrm{PB}})$ and $\Phi_{\mathrm{EH}}(\lambda_{\mathrm{EH}})$ with respective densities $\lambda_{\mathrm{PB}} = \rho\lambda$ and $\lambda_{\mathrm{EH}} = (1-\rho)\lambda$. We assume that an EH is tagged to the PB offering smallest average path loss. It is possible to have multiple EH nodes tagged to the same PB. In case of multiple candidate EH nodes, the PB employs time-division

multiple access (TDMA) to serve all the tagged EHs within the resource block in a round robin fashion. We further assume that the PBs always transmit such that the transmitting PBs constitute a PPP.

Let us consider the case where the PB and EH nodes operate in the mmWave band. Because mmWave signals tend to get blocked by human bodies [54], we treat each node in $\Phi(\lambda)$ as a potential blockage. We call a PB-EH link LOS if it is not intercepted by a blockage. Otherwise, the link is said to be NLOS. We model blockages by combining the approach in [76] with [15], [17]. We represent each blockage as a circle of diameter D. For analytical simplicity, we assume the blockages are drawn from an independent PPP of density λ, despite the fact that they are co-located with the nodes in $\Phi(\lambda)$. We also ignore the possible correlation across the PB-EH links due to common blockages. For a PB-EH link of length r, we define a LOS probability function $p(r) = e^{-\lambda\left(2rD+\frac{\pi D^2}{4}\right)}$, which is the probability that no point of the blockage PPP falls within the rectangular area $2rD$ between the PB and EH (see Fig. 11), or in the semi-circular area $\frac{1}{2}\frac{\pi D^2}{4}$ occupied by the PB and EH bodies [76]. As illustrated in Fig. 11, if the center of a circular blockage falls within the rectangular or the semi-circular regions, the link is assumed to be blocked. Self-body blockage is not considered in this model. Note that it is straightforward to extend the model to urban scenarios, where there could be other potential blockages such as buildings [17].

We now describe the channel model for an arbitrary PB-EH link. Empirical studies suggest that mmWave signals exhibit different propagation characteristics for LOS and NLOS links [53], [54]. We use subscript L (or N) when the serving PB is LOS (or NLOS), and define the link state as $\mathrm{s} \in \{\mathrm{L}, \mathrm{N}\}$. We let $g(r) = C_{\mathrm{s}}/\max(1, r^{\alpha_{\mathrm{s}}})$ denote the distance-dependent attenuation for a PB-EH link of length r, where C_{s} is the path loss intercept, and α_{s} is the path loss exponent. We assume that each link undergoes Nakagami fading, i.e., the channel power gain $H \sim \mathrm{Ga}(N_{\mathrm{s}}, 1/N_{\mathrm{s}})$ follows a normalized Gamma distribution with shape N_{s} and scale $1/N_{\mathrm{s}}$. We leverage the sectored antenna model [37] to capture the use of directional antenna arrays at the PB and EH nodes. Specifically, $\{M_{\mathrm{PB}}, M_{\mathrm{EH}}\}$ give the main lobe gain and $\{m_{\mathrm{PB}}, m_{\mathrm{EH}}\}$ the side lobe gain at the PB and EH. Similarly, $\{\Theta_{\mathrm{PB}}, \Theta_{\mathrm{EH}}\}$ and $\{\theta_{\mathrm{PB}}, \theta_{\mathrm{EH}}\}$ denote the (double-sided) half-power beamwidths for the main and side lobes, respectively. With perfect beam alignment between an EH and its serving PB, it follows that the directivity gain $G = M_{\mathrm{PB}}M_{\mathrm{EH}}$. We assume that the other PBs are randomly oriented with respect to the EH under consideration. For the links from the remaining PBs, we therefore model the directivity gain as a random variable $\mathcal{G}$ with support $\{M_{\mathrm{PB}}M_{\mathrm{EH}}, M_{\mathrm{PB}}m_{\mathrm{EH}}, m_{\mathrm{PB}}M_{\mathrm{EH}}, m_{\mathrm{PB}}m_{\mathrm{EH}}, 0\}$ and corresponding probability masses $\{q_{\mathrm{PB}}q_{\mathrm{EH}}, q_{\mathrm{PB}}\bar{q}_{\mathrm{EH}}, \bar{q}_{\mathrm{PB}}q_{\mathrm{EH}}, \bar{q}_{\mathrm{PB}}\bar{q}_{\mathrm{EH}}, q_0\}$, where $q_{\mathrm{PB}} = \frac{\Theta_{\mathrm{PB}}}{2\pi}$, $\bar{q}_{\mathrm{PB}} = \frac{\theta_{\mathrm{PB}}}{2\pi}$, $q_{\mathrm{EH}} = \frac{\Theta_{\mathrm{EH}}}{2\pi}$, $\bar{q}_{\mathrm{EH}} = \frac{\theta_{\mathrm{EH}}}{2\pi}$, and $q_0 = 2 - q_{\mathrm{PB}} - \bar{q}_{\mathrm{PB}} - q_{\mathrm{EH}} - \bar{q}_{\mathrm{EH}}$ [37]. Note that q_0 is the probability that an EH and a PB are completely misaligned.

B. Key Results: Wireless Energy Transfer in mmWave Tactical Networks

We now introduce the metrics used for characterizing the performance of the considered mmWave system. We leverage Slivnyak's theorem [31] and conduct the analysis at a typical EH located at the origin. Let us denote the received signal power at the origin (in a given time-frequency slot) as $Y = \sum_{x_\ell \in \Phi_{\mathrm{PB}}(\lambda_{\mathrm{PB}})} P_{\mathrm{PB}} D_\ell H_\ell g_\ell(r_\ell)$, where x_ℓ is the ℓth point in Φ_{PB}. We model the corresponding harvested power as $\gamma_{\mathrm{EH}} = \eta_{\mathrm{EH}} Y \mathbb{1}_{\{Y > \psi_{\mathrm{EH}}\}}$, where η_{EH} is the conversion efficiency and ψ_{EH} is the activation threshold of the harvester. When an EH is not being served by its tagged PB, the power harvested from the ambient received signals is negligibly small

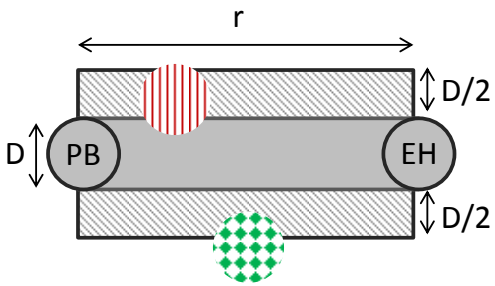

Fig. 11: The illustration shows a mmWave PB and EH (solid circles) separated by a distance r. The red node (vertical pattern) is a potential blocker to a possible LOS PB-EH link whereas the green node (diamond pattern) is not. Each node (blockage) is modeled by a circle of diameter D.

relative to the contribution from the serving PB. We, therefore, focus on the case when the typical EH is being served by its tagged PB. For a required power threshold T, we define $\mathrm{P_{ec}} = \Pr\left[\gamma_{\mathrm{EH}} > \mathrm{T}\right]$ as the energy coverage probability for the typical PB-EH link. We note that the energy coverage probability does not incorporate the potential competition among multiple EHs vying for the same PB. In case of multiple EHs tagged to the same PB, each EH will harvest lesser energy as the (time/frequency) resources are split among all the EHs (e.g., due to TDMA). We also consider a network-level metric $\mathrm{P_{suc}}$ called the success probability which gives the energy coverage probability while taking the EH load into account. We let $N_{\mathrm{suc}} = \lambda_{\mathrm{EH}}\mathrm{P_{suc}}$ denote the average number of successful EHs per unit area.

Energy Coverage Probability: The following proposition characterizes the energy coverage probability in a mmWave tactical network with human-body blockages.

Proposition 3. The energy coverage probability in a mmWave network of density λ, PB fraction ρ, transmit power P_{PB}, and power threshold T can be expressed as

$$\mathrm{P_{ec}}\left(\lambda, P_{\mathrm{PB}}, \rho, \mathrm{T}\right) = \sum_{\mathrm{s}\in\{\mathrm{L},\mathrm{N}\}} \mathrm{P_{ec|s}}\left(\lambda, P_{\mathrm{PB}}, \rho, \hat{\mathrm{T}}\right) A_{\mathrm{s}} \tag{117}$$

where $\hat{\mathrm{T}} = \max\left(\frac{\mathrm{T}}{\eta_{\mathrm{EH}}}, \psi_{\mathrm{EH}}\right)$ is the effective threshold which accounts for the EH efficiency and the activation threshold. For $\mathrm{s} \in \{\mathrm{L}, \mathrm{N}\}$, $\mathrm{P_{ec|s}}\left(\lambda, P_{\mathrm{PB}}, \rho, \hat{\mathrm{T}}\right)$ denotes the conditional energy coverage probability given the state s of the serving link. It is given by

$$\mathrm{P_{ec|s}}\left(\lambda, P_{\mathrm{PB}}, \rho, \hat{\mathrm{T}}\right) \approx K_{\mathrm{s}} + \int_1^{\infty} Q\left(N_{\mathrm{s}}, \frac{\hat{\mathrm{T}} N_{\mathrm{s}} r^{\alpha_{\mathrm{s}}}}{P_{\mathrm{PB}} G C_{\mathrm{s}}}\right) \hat{f}_{\mathrm{s}}(r)\mathrm{d}r, \tag{118}$$

where $K_{\mathrm{s}} = Q\left(N_{\mathrm{s}}, \frac{\hat{\mathrm{T}} N_{\mathrm{s}}}{P_{\mathrm{PB}} G C_{\mathrm{s}}}\right) \int_0^1 \hat{f}_{\mathrm{s}}(r)\mathrm{d}r$, $Q\left(K, x\right) = \frac{\Gamma(K,x)}{\Gamma(K)}$, $\Gamma\left(K, x\right) = \int_x^{\infty} t^{K-1} e^{-t}\mathrm{d}t$ is the upper incomplete Gamma function, and $\Gamma\left(K\right) = \Gamma\left(K, 0\right)$ is the Gamma function.

Proof. See [36]. □

We note that the term K_{s} in (118) accounts for the case where the serving PB lies within a unit circle of the EH, whereas the integral term corresponds to the case where it is located outside. The impact of human-body blockages is captured by the terms A_{s} and $\hat{f}_{\mathrm{s}}(r)$. We note

that the energy coverage probability is dominated by the LOS serving PB because (i) A_{L} is usually much greater than A_{N} for practically relevant values of network density λ and blockage diameter D, and (ii) the contribution from remaining PBs is much smaller than the serving PB due to random beam orientations. Moreover, Proposition 3 is expressed as an integral of a Gamma function, which can be readily computed using numerical tools. Despite its simplicity, the proposed approximation only causes a minor loss in accuracy thanks to directional transmission. Similar to [34], [37], it is possible to obtain a more accurate expression for the energy coverage probability by also considering the other PBs. This, however, comes at the expense of analytical tractability.

Success Probability: We now characterize the success probability which gives the energy coverage probability while incorporating the EH load at the serving PB. In a mmWave (or even UHF) network, the exact characterization of the success probability is challenging since the area distribution of the PB association region is not known. This, in turn, makes it challenging to find the distribution of the EH load (i.e., the number of EHs tagged to a typical PB). Under some simplifying assumptions, we use the following approximation for the EH load distribution at a typical PB.

Lemma 5. *(Modified from [63])* In the considered PPP network with PB fraction ρ, the probability that the PB serving a typical EH has k (where $k \geq 1$) EHs tagged to it, can be approximated as

$$\mathrm{P}_{\mathrm{load}}\left[k,\rho\right] \approx \frac{3.5^{3.5}}{(k-1)!}\frac{\Gamma\left(k+3.5\right)}{\Gamma\left(3.5\right)}\left(\frac{1-\rho}{\rho}\right)^{k-1}\left(3.5+\frac{1-\rho}{\rho}\right)^{-(k+3.5)} \tag{119}$$

We note from Lemma 5 that the load distribution in (119) is determined by the PB fraction ρ, rather than the absolute densities of the PB and EH nodes. Leveraging Lemma 5, we now provide an analytical approximation for the success probability.

Proposition 4. The success probability in a mmWave network of density λ, PB fraction ρ, transmit power P_{PB}, and power threshold T, is given by

$$\mathrm{P}_{\mathrm{suc}}\left(\lambda,\mathrm{P}_{\mathrm{PB}},\rho,\mathrm{T}\right) = \sum_{k=1}^{\infty}\mathrm{P}_{\mathrm{load}}\left[k,\rho\right]\mathrm{P}_{\mathrm{ec}}\left(\lambda,\frac{P_{\mathrm{PB}}}{k},\rho,\mathrm{T}\right), \tag{120}$$

where $\mathrm{P}_{\mathrm{load}}\left[k,\rho\right]$ follows from Lemma 5 and $\mathrm{P}_{\mathrm{ec}}\left(\cdot\right)$ from Proposition 3.

Proof. See [36]. □

We note that truncating the infinite summation in (120) to a few terms (e.g., < 10) results in only a minor loss in accuracy. We also note that when ρ is large, the success probability tends to approach the energy coverage probability. This is because the EHs are less likely to compete over the same PB, suggesting that the performance is mainly limited by the energy transfer link.

Comment: The analytical results in this subsection allow us to calculate the fraction of EH nodes in the network that can successfully harvest sufficient energy to power their operations. This quantity depends on the system parameters such the PB and EH node densities, PB transmit power, EH energy requirement, array size at the PB/EH, and channel parameters.

C. Intuition Obtained

First, increasing the network density improves the energy coverage probability as well as the success probability, despite an increase in human-body blockages. This is because network

densification shortens the link distances, which compensates for the increased blockage density. Second, for a fixed overall node density, there is an optimal PB density that maximizes the average number of successful EHs per unit area. Finally, the results reveal that mmWave may potentially outperform UHF despite blockages due to highly directional transmission.

VII. Wireless Communication with Short Packets

Because remotely-powered communications will feature short packets, the capacity analyses conducted in the asymptotic blocklength regime are not applicable. This has spurred research characterizing the performance of an energy harvesting communication system in the non-asymptotic or finite blocklength regime [23], [27], [45], [81]. Leveraging the finite-length information theoretic framework proposed in [48], [81] characterized the achievable rate for a noiseless binary communications channel with an energy harvesting transmitter. This work was extended to the case of additive white Gaussian noise (AWGN) channel and more general discrete memoryless channels in [23]. For an energy harvesting transmitter operating under a save-then-transmit protocol [47], the achievable rate at the receiver was characterized in the finite blocklength regime [23]. The authors in [27] investigated the mean delay of an energy harvesting channel in the finite blocklength regime. Unlike the work in [23], [27], [81] which assume an infinite battery at the energy harvester, [45] conducted a finite-blocklength analysis for the case of a battery-less energy harvesting channel. Our work differs from prior work on several accounts. The prior work [23], [27], [45], [81] treating short packets falls short of characterizing the performance for the case of wireless energy harvesting. Moreover, most prior work [23], [27], [45], [47], [81] implicitly assumes concurrent harvest and transmit operation, which may be infeasible in practice. While the previous work focuses on isolated setups, we leverage a stochastic geometry framework to study a wireless-powered communication network with short packets.

A. Model for Wireless-powered Communications with Short Packets

We consider a wireless-powered communication system where one or more wireless power beacons (PBs) use wireless energy transfer to charge an energy harvesting (EH) node, which then attempts to communicate with another receiver (RX) using the harvested energy (see Fig. 9). Previously, we presented an analytical treatment for a three-node setup where the energy harvesting node is powered by a single power beacon. We now extend the analysis to a large-scale network consisting of power beacons, wireless-powered transmitters, and their dedicated receivers. A potential application is tactical sensor networks where the communicating sensors are remotely-powered by power beacons. We assume that the power beacons are distributed on a two-dimensional plane according to a homogeneous PPP $\Phi_{\mathrm{PB}} = \{x_k\}_{k=1}^{\infty}$ with density (intensity) λ_{PB}, where x_k denotes the location of a node k in Φ_{PB}. The energy harvesting transmitters are drawn from another homogeneous PPP $\Phi_{\mathrm{EH}} = \{y_k\}_{k=1}^{\infty}$ of density λ_{EH} independently of the power beacons. Similar to the case of a single power beacon, each energy harvesting transmitter is assumed to have a dedicated receiver located a fixed distance away. Leveraging Slivnyak's theorem [31], we consider a typical energy harvesting node located at the origin. It exploits the energy harvested from the transmissions of power beacons to communicate with its dedicated receiver amid interference and noise.

We assume that the energy harvester uses a *save-then-transmit* protocol [47] to enable wireless-powered communications. The considered protocol divides the communication frame consisting of S channel uses (or slots) into an energy harvesting phase having m channel uses, and an

information transmission phase having n channel uses. The first m channel uses are used for harvesting energy from the RF signals transmitted by the power beacons. This is followed by an information transmission phase consisting of n channel uses, where the transmitter uses the harvested energy to transmit information to the receiver. We assume that any left-over energy at the end of the transmission is stored in a dedicated battery for system-level energy supply. For example, this dedicated battery may support other functions like sensing and computation, which an EH node often needs to perform. This implies that the energy accumulated in a harvesting phase is independent of the previous harvesting phases. We leave the case where left-over energy supports subsequent transmissions for future work. We call m the *harvest* blocklength, n the *transmit* blocklength, and $S = m + n$ the *total* blocklength or frame size. We will conduct the subsequent analysis for the non-asymptotic blocklength regime, i.e., for the practical case of *short packets* where the total blocklength is finite.

Energy Harvesting Phase: The signal transmitted by a power beacon experiences distance-dependent path loss and channel fading before reaching the energy harvesting node. The harvested energy is, therefore, a random quantity due to the underlying randomness of the wireless link. We let random variable Z_i model the power (or energy) harvested in slot i ($i = 1, \cdots, m$). We let h_k model the small-scale fading coefficient for the PB-EH link originating from the PB located at x_k. We assume IID Rayleigh fading for the PB-EH links such that $H_k = |h_k|^2 \sim \mathrm{Exp}\,(1)$. The energy harvested in an arbitrary channel use is given by $Z = P_{\mathrm{PB}}\mu\tilde{Z}$, where $\tilde{Z} = \sum\limits_{x_k \in \Phi_{\mathrm{PB}}} \frac{H_k}{\ell(\|x_k\|,\eta)}$, where $\mu \in (0, 1]$ denotes the EH conversion efficiency, P_{PB} is the PB transmit power (i.e., energy per PB symbol), $\ell\left(\|x_k\|, \eta\right)$ gives the distance-dependent path loss given a PB-EH link distance $\|x_k\|$ and a path loss exponent $\eta > 2$. We let $Z_{\mathrm{tot}} = \sum_{i=1}^{m} Z_i$ denote the total harvested energy during a harvesting phase. Note that we have ignored the energy due to noise since it is negligibly small. We assume the PB-EH link undergoes quasi-static block flat fading where the channel remains constant over (the harvesting phase of) a frame, and randomly changes to a new value for the next frame. This means that the energy arrivals within a harvesting phase are fully correlated, i.e., $Z_i = Z_1 \triangleq Z$, $\forall\, i = 1, 2, \cdots, m$ such that $Z_{\mathrm{tot}} \sim \mathrm{Ga}(1, mP_{\mathrm{H}})$. This is motivated by the observation that the harvest blocklength in a *short-packet* communication system may be smaller than the channel coherence time.

Information Transmission Phase: The energy harvesting phase is followed by an information transmission phase where the EH node attempts to communicate with a destination RX node over an unreliable AWGN channel. The AWGN channel abstracts a scenario where the EH-RX channel remains fairly static, for example, due to a small link distance. Contrary to the harvesting operation, here noise plays a significant role. We assume that the EH node uses a Gaussian codebook for signal transmission. We let X_ℓ be the signal intended for transmission in slot ℓ with an average power P_{EH}, where $\ell = 1, \cdots, n$, and n is fixed. In the ensuing analysis, we assume P_{EH} to be fixed before evaluating the considered metrics. The resulting (intended) sequence $X^n = (X_1, \cdots, X_n)$ consists of independent and identically distributed (IID) Gaussian random variables such that $X_\ell \sim \mathcal{N}(0, P_{\mathrm{EH}})$. To transmit the intended sequence X^n over the transmit block, the EH node needs to satisfy the energy constraints in (80). The following lemma simplifies the multiple energy constraints into a single constraint.

Lemma 6. For a random sequence $\{X_\ell\}_{\ell=1}^{n}$ for the transmit phase, and a random energy sequence $\{Z_i\}_{i=1}^{m}$ for the harvest phase, the probability of violating the energy constraints in (80) is given

by

$$\Pr\left[\bigcup_{k=1}^{n}\left\{\sum_{\ell=1}^{k}X_\ell^2>\sum_{i=1}^{m}Z_i\right\}\right]=1-\Pr\left[\sum_{\ell=1}^{n}X_\ell^2\leq\sum_{i=1}^{m}Z_i\right]. \tag{121}$$

Proof. See [39]. □

The constraints in (80), which need to be satisfied to transmit the intended codeword, simplify to $\sum_{\ell=1}^{n}X_\ell^2\leq Z_{\rm tot}$ due to Lemma 6. We let $\tilde{X}^n=\left(\tilde{X}_1,\cdots,\tilde{X}_n\right)$ be the transmitted sequence. Note that $\tilde{X}^n\neq X^n$ when the energy constraints are violated as the EH node lacks sufficient energy to put the intended symbols on the channel. The signal received at the destination node in slot ℓ is given by $Y_\ell=\tilde{X}_\ell+V_\ell$, where $V^n=(V_1,\cdots,V_n)$ is an IID sequence modeling the receiver noise such that $V_\ell\sim\mathcal{N}(0,\sigma^2)$ is a zero-mean Gaussian random variable with variance σ^2. We note that any deterministic channel gain (attenuation) $\zeta\in(0,1]$ for the EH-RX link can be equivalently tackled by scaling the noise variance by a factor ζ (as the equivalent channel is still AWGN). Similarly, we define $Y^n=(Y_1,\cdots,Y_n)$ as the received sequence.

B. Key Results: Wireless-powered Communications with Short Packets

We now introduce the metrics used for characterizing the performance of the considered *short-packet* wireless-powered communications system. The overall performance of the considered system is marred by two error events. First, due to lack of sufficient energy, the EH node may not be able to transmit the intended codewords during the information transmission phase, possibly causing a decoding error at the receiver. Second, due to a noisy EH-RX channel, the received signal may not be correctly decoded. For the former, we define a metric called the *energy supply probability*, namely, the probability that an EH node can support the intended transmission. For the latter, we define and characterize the ϵ*-achievable rate* in the finite blocklength regime.

Energy Supply Probability: We first characterize the energy supply probability in a general form. We then specialize it to the scenario considered in the system model.

Proposition 5. For the case of multiple power beacons with PB density $\lambda_{\rm PB}$, the energy supply probability at a typical EH node is given by

$$P_{\rm es}^{\rm MP}\left(m,n,a,\lambda_{\rm PB},\eta\right)=1-\sum_{i=0}^{\frac{n}{2}-1}(-1)^i\frac{m^i}{(2a)^i i!}\frac{\mathrm{d}^i}{\mathrm{d}s^i}\mathcal{L}_{\tilde{Z}}(s)|_{s=\frac{m}{2a}} \tag{122}$$

where the power ratio $a=\frac{P_{\rm EH}}{\mu P_{\rm PB}}$, η is the path loss exponent, while $\mathcal{L}_{\tilde{Z}}(s)=\mathbb{E}[e^{-s\tilde{Z}}]$ is the Laplace transform of $\tilde{Z}$, which is a function of $\lambda_{\rm PB}$ and η.

Proof. See [39]. □

Note that the power ratio a is defined as the ratio of the transmit power at an energy harvester to that at a power beacon (scaled by the rectifier efficiency). For generality, we have expressed Proposition 5 in terms of the Laplace transform of the harvested energy. Depending on the propagation and network model, this could be evaluated in closed form. For example, the following lemma analytically characterizes the Laplace transform for the scenario considered.

Lemma 7. Let us assume the PBs are drawn from a homogeneous PPP of density $\lambda_{\rm PB}$, the PB-EH links are IID Rayleigh fading, and follow a bounded path loss model $\ell(r,\eta)=\max(1,r^\eta)$

where $\eta > 2$ is the path loss exponent while r is the PB-EH link distance. The Laplace transform $\mathcal{L}_Z(s)$ of the per-slot harvested energy Z is analytically characterized by

$$\mathcal{L}_Z(s) = \exp\left(-\pi\lambda_{\mathrm{PB}}\frac{P_{\mathrm{PB}}\mu s}{1+P_{\mathrm{PB}}\mu s}\right)\exp\left(-\pi\lambda_{\mathrm{PB}}\ \mathcal{F}\left(P_{\mathrm{PB}}\mu s,\eta\right)\right), \tag{123}$$

where the function $\mathcal{F}\left(x_1,x_2\right)$ for $x_1 \geq 0, x_2 > 2$ is defined as

$$\mathcal{F}\left(x_1,x_2\right) = \frac{2x_1}{x_2-2}\ {}_2F_1\left(1,1-\frac{2}{x_2};2-\frac{2}{x_2};-x_1\right) \tag{124}$$

in terms of the Gauss's hypergeometric function ${}_2F_1\left(c_1,c_2\,;c_3\,;z\right)$ [49]. The Laplace transform $\mathcal{L}_{\tilde{Z}}(s)$ is a special case of (123), which is obtained by plugging $P_{\mathrm{PB}}\mu = 1$.

Proof. See [39]. □

We note that the Laplace transform is expressed in terms of tractable mathematical functions, which can be evaluated using most numerical toolboxes. We now characterize the mean harvested energy in terms of the network density and the path loss exponent.

Lemma 8. The average per-slot harvested energy for the case of multiple power beacons is given by $\mathbb{E}\left[Z\right] = \lambda_{\mathrm{PB}}\pi\frac{\eta}{\eta-2}\mu P_{\mathrm{PB}}$. This shows that the λ_{PB} and P_{PB} have the same effect on the mean harvested energy.

Proof. See [39]. □

In the following proposition, we propose an approximate expression to simplify the computation of the energy supply probability.

Proposition 6. The energy supply probability for the case of multiple power beacons can be approximated as

$$P_{\mathrm{es}}^{\mathrm{MP}}\left(m,n,a,\lambda_{\mathrm{PB}},\eta\right) \approx 1 - F_{\tilde{Z}}\left(\frac{an}{m}\right), \tag{125}$$

where $F_{\tilde{Z}}\left(\cdot\right)$ can be evaluated using the numerical inversion technique of Lemma 9, aided by the Laplace transform characterization of Lemma 7.

Proof. See [39]. □

We now present an analytical expression to evaluate $F_{\tilde{Z}}(\cdot)$ using numerical inversion.

Lemma 9. Let us define positive constants A, B and C. We can evaluate $F_{\tilde{Z}}(x)$ using

$$F_{\tilde{Z}}(x) = \frac{2^{-B}e^{\frac{A}{2}}}{x}\sum_{b=0}^{B}\binom{B}{b}\sum_{c=0}^{C+b}\frac{(-1)^c}{D_c}\ \mathrm{Re}\left[\frac{\mathcal{L}_{\tilde{Z}}(s)}{s}\right], \tag{126}$$

where $s = \frac{A+j2\pi c}{2x}$, $D_c = 2$ when $c = 0$ and $D_c = 1$ when $c \in \{1,2,\cdots,C+b\}$, $\mathrm{Re}[\cdot]$ denotes the real part, and $\mathcal{L}_{\tilde{Z}}(s)$ follows from Lemma 7.

Proof. See [5], [40] □

With parameters A, B and C chosen carefully, the finite summation in (126) yields stable numerical inversion with a bounded estimation error. To obtain a solution correct to $\varrho-1$ decimal places, these parameters should satisfy $A \geq \varrho\log(10)$, $B \geq 1.243\varrho - 1$ and $C \geq 1.467\varrho$ [5], [28], [40].

Achievable Rate: We now characterize the ergodic achievable rate for the case of multiple power beacons. We also account for the network interference due to other EH transmitters. Let us consider a typical receiver at the origin, which receives useful signal from its dedicated EH transmitter over an AWGN channel, and interference from the other EH nodes over possibly fading links. This is a potential scenario as the dedicated EH-RX link distance could be much smaller than that from an interferer. For analytical simplicity, we assume that the interfering links undergo quasi-static fading such that the channels remain static over the entire codeword. We define g_k as the small-scale fading coefficient for the link originating from the EH transmitter at y_k. We assume IID Rayleigh fading for the interfering links such that $G_k = |g_k|^2 \sim \text{Exp}\,(1)$. Similar to the serving EH, an interfering EH transmits independent symbols from a Gaussian codebook with an average transmit power P_{EH} during the transmit phase. We define $I = \sum_{y_k \in \Phi_{\text{EH}}, k \neq 0} \frac{P_{\text{EH}} G_k}{\ell(\|y_k\|, \eta)}$ as the aggregate interference power and $\gamma_I = \frac{\zeta P_{\text{EH}}}{\sigma^2 + I}$ as the signal-to-interference-plus-noise ratio (SINR) at the typical receiver, where the constant $\zeta \in (0, 1]$ models any (deterministic) attenuation for the serving link, known to the transmitter and receiver. We further assume that interference is treated as noise for the purpose of decoding. We first characterize the Laplace transform of I, which is then used for evaluating the CDF $F_I(\cdot)$ using numerical inversion.

Lemma 10. The Laplace transform $\mathcal{L}_I(s)$ of the interference I is analytically characterized by

$$\mathcal{L}_I(s) = \exp\left(-\pi \lambda_{\text{EH}} \frac{P_{\text{EH}} s}{1 + P_{\text{EH}} s}\right) \exp\left(-\pi \lambda_{\text{EH}}\, \mathcal{F}\left(P_{\text{EH}} s, \eta\right)\right), \tag{127}$$

where $\mathcal{F}\left(\cdot, \cdot\right)$ follows from (124).

Proof. See [39]. □

Theorem 8. In a large-scale network with PB density λ_{PB}, EH density λ_{EH}, PB transmit power P_{PB}, EH transmit power P_{EH}, the ergodic non-asymptotic ϵ-achievable rate at a typical receiver is characterized by

$$R_{\text{EH}}^{\text{MP}}\left(\epsilon, a, P_{\text{PB}}, P_{\text{EH}}, m, n, \lambda_{\text{PB}}, \lambda_{\text{EH}}\right) = \frac{\frac{n}{2}\mathbb{E}_I\left[\log(1 + \gamma_I)\right] - \sqrt{\frac{2+\epsilon}{\epsilon} n}\mathbb{E}_I\left[\sqrt{\frac{\gamma_I}{\gamma_I + 1}}\right] - (n)^{\frac{1}{4}} - 1}{n + m}, \tag{128}$$

where

$$\mathbb{E}_I\left[\log\left(1 + \gamma_I\right)\right] = \int_0^{\tau} F_I\left(\frac{\zeta P_{\text{EH}}}{e^t - 1} - \sigma^2\right) \mathrm{d}t \tag{129}$$

for $\tau = \log\left(1 + \zeta\gamma\right)$,

$$\mathbb{E}_I\left[\sqrt{\frac{\gamma_I}{\gamma_I + 1}}\right] = \int_0^{\hat{\tau}} F_I\left(\zeta P_{\text{EH}}\left(\frac{1}{t^2} - 1\right) - \sigma^2\right) \mathrm{d}t \tag{130}$$

for $\hat{\tau} = \sqrt{\frac{1}{1 + \frac{1}{\zeta\gamma}}}$, and $F_I(\cdot)$ can be evaluated using Lemma 9. The expression in (128) holds for all tuples (m, n) satisfying the constraints in (131) and (132), i.e.,

$$n \geq \left\lceil \log\left(\frac{2 + \epsilon}{\epsilon^2}\right)\right\rceil^4 \tag{131}$$

and

$$\sum_{i=0}^{\frac{n}{2}-1}(-1)^i\frac{m^i}{(2a)^i i!}\frac{\mathrm{d}^i}{\mathrm{d}s^i}\mathcal{L}_{\tilde{Z}}(s)\bigg|_{s=\frac{m}{2a}} \leq \frac{\epsilon}{2+\epsilon} \tag{132}$$

where $\mathcal{L}_{\tilde{Z}}(s)$ follows from Lemma 7.

Proof. See [39]. □

Here, (131) specifies the minimum transmit blocklength required for the target ϵ. Similarly, given n and a, (132) ensures that the harvest blocklength is large enough such that the energy outage probability is bounded by $\frac{\epsilon}{2+\epsilon}$ (and the target error probability by ϵ). The impact of other parameters such as the PB density and the path loss exponent is captured by $\mathcal{L}_{\tilde{Z}}(s)$. Eq. (132) can be evaluated using the expression derived for the Laplace transform. We note that the Poisson network of PBs impacts the energy outage probability, which is captured in (132). The Poisson network of EHs generates interference hurting the communication link, which is accounted for in (128). Further, the *ergodic* achievable rate in (128) is obtained by averaging over the aggregate interference, i.e., interferer locations and small-scale fading.

Comment: The analytical results presented in this subsection allow us to calculate the achievable rate in a wireless-powered large-scale communication network with short packets. The rate depends on various system parameters such as the PB/EH node densities, duration of the energy harvesting/data transmission phases, and the reliability requirement of the communication system.

C. Intuition Obtained

The results provide additional insights on the performance of remotely-powered communication systems with short packets. They show that increasing the PB node density is more beneficial for the system performance than increasing the PB transmit power. Furthermore, the data rate is sensitive to the transmit/harvest blocklengths, confirming that the insights obtained from an asymptotic blocklength analysis are not applicable to a wireless-powered network with short packets.

VIII. Itemized Summary of All Results

- Derivation of the SINR CCDF of a mmWave ad hoc network in LOS and NLOS communication incorporating building blockage and directional antennas [66], [67]. This revealed the importance of LOS communication in ad hoc networks.
- Computation of the transmission capacity and area spectral efficiency of the network [66], [67]. This work shows how different transmission parameters like beamwidth, user density, and building density impact network wide performance.
- Derivation of a general expression for the INR of a mmWave ad hoc network [66], [66]. This has several implications on network design [66], [66], for example if a user density causes interference-limited operation, the network initiates interference mitigation schemes.
- Development of the two-way transmission capacity which adds a requirement of a reverse link to support low-rate acknowledgment messages [66]. This allows optimal resource allocation based on rate requirements and transmission success rate.
- Formulation of the average sum rate, ergodic capacity, of the users in a mmWave ad hoc network [70] which captures the trade-off between per user rate and overall network efficiency.

- Establishing the loss in ergodic capacity due to antenna array direction misalignment assuming Gaussian error [70]. This gives a metric to measure the overall network value of a training scheme based to the error of the algorithm.
- Derivation of the ergodic capacity of uniform ad hoc networks [72]. This revealed further verification that mmWave ad hoc networks are interference limited.
- Computation of the ergodic capacity for clustered mmWave ad hoc networks [71], [72]. This work shows how mmWave networks effectively deal with intra-cluster interference because of the reduced interference at mmWave frequencies.
- Derivation of a scaling law for mmWave ad hoc networks [69], [72]. This shows the sub-linear relationship between antenna array size and transmitter density with regards to ergodic capacity.
- Analysis of the energy supply probability for mmWave ad hoc networks [38]. This shows how often and probable the energy needed for transmission will be available.
- Computation of the achievable rate in energy harvesting networks [38]. This gives intuition on the optimal transmit power given energy harvesting parameters.
- Derived and defined a framework, the intra-ϵ inter-cluster coverage, that balances between the data rate within a user cluster while maintaining communication between user clusters. The results indicate that, for small cluster radii, communication between user clusters can occur if the required data rate is not too large.
- Computed the average overhead of three beamforming methods and their affect on ergodic rate. The results show that for ad hoc networks, contrary to cellular networks, simultaneous exhaustive search may be necessary to overcome interference and path-loss of mmWave communication.
- Developed a framework to characterize the performance of wireless power transfer in a tactical mmWave ad hoc network while taking blockage due to soldier bodies into account [35], [36]. Derived energy coverage probability which measures the fraction of successful power transfer links in the ad hoc network. Results show that mmWave gives better energy coverage compared to lower-frequency solutions.
- Discovered a tradeoff between the number of remotely powered nodes and the number of power beacon nodes in a tactical network. The analysis reveals a key design insight that deploying roughly half of the network nodes as power beacons maximizes the number of successful energy harvesting nodes.
- Extended the analytical framework developed in the earlier phases for modeling remotely-powered communication with short packets. Derived the energy supply probability and the achievable rate in a network setting where multiple power transmitters charge energy harvesting sensors to enable them to communicate information to their intended receivers. The derived expressions relate the energy supply probability and the achievable rate for reliable communication with system parameters such as the transmitter density, transmit power, energy harvesting duration and data transmission duration.

REFERENCES

[1] D5.1 Channel Modeling and Characterization. [Online]. Available: http://www.miweba.eu/wp-content/uploads/2014/07/MiWEBA_D5.1_v1.011.pdf

[2] IEEE P802.11 - Task Group ay. [Online]. Available: http://www.ieee802.org/11/Reports/tgay_update.htm

[3] Strategic spectrum plan. [Online]. Available: http://1.usa.gov/223bNL5

[4] "IEEE Standard for Information technology–Telecommunications and information exchange between systems–Local and metropolitan area networks–Specific requirements-Part 11: Wireless LAN Medium Access Control (MAC) and Physical Layer (PHY) Specifications Am," pp. 1–628, 2012.

[5] J. Abate and W. Whitt, "Numerical inversion of Laplace transforms of probability distributions," *ORSA Journal on computing*, vol. 7, no. 1, pp. 36–43, 1995.

[6] A. Alkhateeb, O. El Ayach, G. Leus, and R. Heath, "Hybrid precoding for millimeter wave cellular systems with partial channel knowledge," in *Information Theory and Applications Workshop (ITA), 2013*, 2013, pp. 1–5.

[7] A. Alkhateeb, Y. H. Nam, M. S. Rahman, C. Zhang, and R. Heath, "Initial beam association in millimeter wave cellular systems: Analysis and design insights," *IEEE Transactions on Wireless Communications*, vol. PP, no. 99, pp. 1–1, 2017.

[8] J. Andrews *et al.*, "Rethinking information theory for mobile ad hoc networks," *IEEE Commun. Mag.*, vol. 46, no. 12, pp. 94–101, 2008.

[9] J. Andrews, S. Shakkottai, R. Heath, N. Jindal, M. Haenggi, R. Berry, D. Guo, M. Neely, S. Weber, S. Jafar, and A. Yener, "Rethinking information theory for mobile ad hoc networks," *IEEE Commun. Mag.*, vol. 46, no. 12, pp. 94–101, 2008.

[10] F. Baccelli and B. Blaszczyszyn, *Stochastic Geometry and Wireless Networks, Volume I - Theory*. NoW Publishers, 2009, vol. 1. [Online]. Available: http://hal.inria.fr/inria-00403039

[11] ——, *Stochastic Geometry and Wireless Networks, Volume II - Applications*. NoW Publishers, 2009, vol. 2. [Online]. Available: http://hal.inria.fr/inria-00403040

[12] T. Bai and R. W. Heath Jr., "Coverage and rate analysis for millimeter wave cellular networks," *IEEE Trans. Wireless Commun.*, Feb 2015, Available Online: http://arxiv.org/abs/1402.6430.

[13] T. Bai, R. Vaze, and R. W. Heath Jr., "Analysis of Blockage Effects on Urban Cellular Networks," *IEEE Trans. Wireless Commun.*, vol. 13, no. 9, pp. 5070–5083, Sept 2014.

[14] T. Bai, A. Alkhateeb, and R. W. Heath Jr., "Coverage and capacity of millimeter-wave cellular networks," *IEEE Communications Magazine*, vol. 52, no. 9, pp. 70–77, September 2014.

[15] T. Bai and R. Heath, "Coverage and rate analysis for millimeter-wave cellular networks," *IEEE Trans. Wireless Commun.*, vol. 14, no. 2, pp. 1100–1114, Feb. 2015.

[16] T. Bai and R. W. H. Jr., "Coverage analysis in dense millimeter wave cellular networks," in *Proc. of 47th Asilomar Conference on Signals, Systems and Computers*, Pacific Grove, CA, Nov. 2013.

[17] T. Bai, R. Vaze, and R. Heath, "Analysis of blockage effects on urban cellular networks," *IEEE Trans. Wireless Commun.*, vol. 13, no. 9, pp. 5070–5083, Sep. 2014.

[18] S. Bellofiore, J. Foutz, R. Govindarajula, I. Bahceci, C. Balanis, A. Spanias, J. Capone, and T. Duman, "Smart antenna system analysis, integration and performance for mobile ad-hoc networks (manets)," *IEEE Trans. Antennas Propag.*, vol. 50, no. 5, pp. 571–581, 2002.

[19] F. Boccardi, R. Heath Jr., A. Lozano, T. Marzetta, and P. Popovski, "Five disruptive technology directions for 5G," *IEEE Commun. Mag.*, vol. 52, no. 2, pp. 74–80, February 2014.

[20] S. N. Chiu, D. Stoyan, W. S. Kendall, and J. Mecke, *Stochastic Geometry and Its Applications*. Wiley, September 2013.

[21] R. Choudhury, X. Yang, R. Ramanathan, and N. Vaidya, "On designing mac protocols for wireless networks using directional antennas," *Mobile Computing, IEEE Transactions on*, vol. 5, no. 5, pp. 477 – 491, may 2006.

[22] O. El Ayach, S. Rajagopal, S. Abu-Surra, Z. Pi, and R. W. Heath, Jr, "Spatially Sparse Precoding in Millimeter Wave MIMO Systems," *submitted to*.

[23] S. L. Fong, V. Y. Tan, and J. Yang, "Non-asymptotic achievable rates for energy-harvesting channels using save-and-transmit," *arXiv preprint arXiv:1507.02444*, 2015.

[24] R. K. Ganti and M. Haenggi, "Interference and Outage in Clustered Wireless Ad Hoc Networks," *IEEE Trans. Inf. Theory*, vol. 55, no. 9, pp. 4067–4086, Sept 2009.

[25] M. Gapeyenko *et al.*, "Analysis of human-body blockage in urban millimeter-wave cellular communications," in *Proc. IEEE Int. Conf. Commun.*, May 2016, pp. 1–7.

[26] R. Gowaikar, B. Hochwald, and B. Hassibi, "Communication over a wireless network with random connections," *IEEE Transactions on Information Theory*, vol. 52, no. 7, pp. 2857–2871, Jul. 2006.

[27] A. Guo, H. Yin, and W. Wang, "Performance analysis of energy harvesting wireless communication system with finite blocklength," *IEEE Commun. Lett.*, vol. 20, no. 2, pp. 324–327, Feb. 2016.

[28] J. Guo, S. Durrani, and X. Zhou, "Outage probability in arbitrarily-shaped finite wireless networks," *IEEE Trans. Commun.*, vol. 62, no. 2, pp. 699–712, 2014.

[29] P. Gupta and P. Kumar, "The capacity of wireless networks," *IEEE Transactions on Information Theory*, vol. 46, no. 2, pp. 388–404, Mar. 2000. [Online]. Available: http://ieeexplore.ieee.org/lpdocs/epic03/wrapper.htm?arnumber=825799

[30] ——, "The capacity of wireless networks," *IEEE Trans. Inf. Theory*, vol. 46, no. 2, pp. 388–404, Mar. 2000.

[31] M. Haenggi, *Stochastic geometry for wireless networks*. Cambridge University Press, 2012.

[32] K. Huang, J. Andrews, D. Guo, R. Heath, and R. Berry, "Spatial interference cancellation for multiantenna mobile ad hoc networks," *IEEE Trans. Inf. Theory*, vol. 58, no. 3, pp. 1660–1676, 2012.

[33] A. Hunter, J. Andrews, and S. Weber, "Transmission capacity of ad hoc networks with spatial diversity," *IEEE Trans. Wireless Commun.*, vol. 7, no. 12, pp. 5058–5071, 2008.

[34] T. A. Khan, A. Alkhateeb, and R. W. Heath, "Energy coverage in millimeter wave energy harvesting networks," in *2015 IEEE Globecom Workshops (GC Wkshps)*, Dec. 2015, pp. 1–6.

[35] T. A. Khan and R. W. Heath, "Wireless power transfer in millimeter wave tactical networks," *IEEE Signal Process. Lett.*, vol. 24, no. 9, pp. 1284–1287, Sep. 2017.

[36] T. Khan and R. W. Heath Jr., "Analyzing Wireless Power Transfer in Millimeter Wave Networks with Human Blockages," in *IEEE Military Communications Conference (MILCOM)*, Oct. 2017 (accepted).

[37] T. A. Khan, A. Alkhateeb, and R. Heath, "Millimeter wave energy harvesting," *IEEE Trans. Wireless Commun.*, vol. 15, no. 9, pp. 6048–6062, Sep. 2016.

[38] T. A. Khan, R. W. Heath, and P. Popovski, "On wirelessly powered communications with short packets," *to appear in IEEE GLOBECOM Workshops*, 2016.

[39] T. A. Khan, R. W. Heath Jr, and P. Popovski, "Wirelessly powered communication networks with short packets," *to appear in IEEE Trans. Commun. arXiv preprint arXiv:1610.07672*, 2017.

[40] Y.-C. Ko, M.-S. Alouini, and M. K. Simon, "Outage probability of diversity systems over generalized fading channels," *IEEE Trans. Commun.*, vol. 48, no. 11, pp. 1783–1787, 2000.

[41] M. Kulkarni, S. Singh, and J. Andrews, "Coverage and rate trends in dense urban mmwave cellular networks," in *Global Communications Conference (GLOBECOM), 2014 IEEE*, Dec 2014, pp. 3809–3814.

[42] N. Lee, F. Baccelli, and R. W. Heath Jr., "Spectral Efficiency Scaling Laws in Dense Random Wireless Networks with Multiple Receive Antennas," *CoRR*, vol. abs/1410.7502, 2014. [Online]. Available: http://arxiv.org/abs/1410.7502

[43] ——, "Spectral Efficiency Scaling Laws in Dense Random Wireless Networks With Multiple Receive Antennas," *IEEE Trans. Inf. Theory*, vol. 62, no. 3, pp. 1344–1359, March 2016.

[44] Y. Li, J. G. Andrews, F. Baccelli, T. D. Novlan, and J. C. Zhang, "Design and analysis of initial access in millimeter wave cellular networks," *CoRR*, vol. abs/1609.05582, 2016. [Online]. Available: http://arxiv.org/abs/1609.05582

[45] E. MolavianJazi and A. Yener, "Low-latency communications over zero-battery energy harvesting channels," in *Proc. of IEEE Global Commun. Conf. (GLOBECOM)*, Dec. 2015, pp. 1–6.

[46] B. Nosrat-Makouei, R. K. Ganti, J. G. Andrews, and R. W. Heath Jr., "MIMO Interference Alignment in Random Access Networks," *IEEE Trans. Commun.*, vol. 61, no. 12, pp. 5042–5055, Dec. 2013.

[47] O. Ozel and S. Ulukus, "Achieving AWGN capacity under stochastic energy harvesting," *IEEE Trans. Inf. Theory*, vol. 58, no. 10, pp. 6471–6483, Oct. 2012.

[48] Y. Polyanskiy, H. V. Poor, and S. Verdu, "Channel coding rate in the finite blocklength regime," *IEEE Trans. Inf. Theory*, vol. 56, no. 5, pp. 2307–2359, May 2010.

[49] A. Prudnikov, *Integrals and series: special functions*.

[50] C. Psomas and I. Krikidis, "Blockage effects on joint information energy transfer in directional ad-hoc networks," in *Proc. 24th European Signal Process. Conf.*, Aug. 2016, pp. 808–812.

[51] R. Ramanathan, J. Redi, C. Santivanez, D. Wiggins, and S. Polit, "Ad hoc networking with directional antennas: a complete system solution," *IEEE J. Sel. Areas Commun.*, vol. 23, no. 3, pp. 496–506, 2005.

[52] D. Ramasamy, S. Venkateswaran, and U. Madhow, "Compressive Parameter Estimation in AWGN," *IEEE Transactions on Signal Processing*, vol. 62, no. 8, pp. 2012–2027, April 2014.

[53] S. Rangan, T. Rappaport, and E. Erkip, "Millimeter-wave cellular wireless networks: Potentials and challenges," *Proc. IEEE*, vol. 102, no. 3, pp. 366–385, Mar. 2014.

[54] T. S. Rappaport, R. W. Heath Jr, R. C. Daniels, and J. N. Murdock, *Millimeter Wave Wireless Communications*. Pearson Education, 2014.

[55] T. S. Rappaport, G. R. MacCartney, M. K. Samimi, and S. Sun, "Wideband Millimeter-Wave Propagation Measurements and Channel Models for Future Wireless Communication System Design," *IEEE Trans. Commun.*, vol. 63, no. 9, pp. 3029–3056, Sept 2015.

[56] T. Rappaport, E. Ben-Dor, J. Murdock, and Y. Qiao, "38 GHz and 60 GHz angle-dependent propagation for cellular amp; peer-to-peer wireless communications," in *Proc. of 2012 IEEE International Conference on Communications (ICC)*, 2012, pp. 4568–4573.

[57] ——, "38 GHz and 60 GHz angle-dependent propagation for cellular amp; peer-to-peer wireless communications," in *Proc. of IEEE International Conference on Communications (ICC)*, Jun 2012, pp. 4568–4573.

[58] T. Rappaport, R. W. Heath Jr., R. C. Daniels, and J. Murdock, *Millimeter Wave Wireless Communications*. Prentice-Hall, September 2014.

[59] T. Rappaport, S. Sun, R. Mayzus, H. Zhao, Y. Azar, K. Wang, G. Wong, J. Schulz, M. Samimi, and F. Gutierrez, "Millimeter Wave Mobile Communications for 5G Cellular: It Will Work!" *IEEE Access*, vol. 1, pp. 335–349, 2013.

[60] ——, "Millimeter Wave Mobile Communications for 5G Cellular: It Will Work!" *IEEE Access*, vol. 1, pp. 335–349, 2013.

[61] J. Singh, S. Ponnuru, and U. Madhow, "Multi-gigabit communication: the adc bottleneck1," in *Ultra-Wideband, 2009. ICUWB 2009. IEEE International Conference on*, 2009, pp. 22–27.

[62] S. Singh, R. Mudumbai, and U. Madhow, "Interference Analysis for Highly Directional 60-GHz Mesh Networks: The Case for Rethinking Medium Access Control," *IEEE/ACM Trans. Netw.*, vol. 19, no. 5, pp. 1513–1527, 2011.

[63] S. Singh, H. S. Dhillon, and J. G. Andrews, "Offloading in heterogeneous networks: Modeling, analysis, and design insights," *IEEE Trans Wireless Commun.*, vol. 12, no. 5, pp. 2484–2497, 2013.

[64] S. Singh, M. N. Kulkarni, A. Ghosh, and J. G. Andrews, "Tractable model for rate in self-backhauled millimeter wave cellular networks," *CoRR*, vol. abs/1407.5537, 2014. [Online]. Available: http://arxiv.org/abs/1407.5537

[65] P. Stoica and N. Arye, "MUSIC, maximum likelihood, and Cramer-Rao bound," *IEEE Transactions on Acoustics, Speech and Signal Processing*, vol. 37, no. 5, pp. 720–741, May 1989.

[66] A. Thornburg, T. Bai, and R. W. Heath, "Performance analysis of outdoor mmwave ad hoc networks," *IEEE Transactions on Signal Processing*, vol. 64, no. 15, pp. 4065–4079, 2016.

[67] A. Thornburg, T. Bai, and R. W. Heath Jr., "Coverage and Capacity of mmWave Ad Hoc Networks," in *Proc. of IEEE International Conference on Communications (ICC)*, Jun 2015.

[68] ——, "Interference Statistics in a Random mmWave Ad Hoc Network," in *Proc. of IEEE ICASSP*, Apr 2015.

[69] A. Thornburg, R. Daniels, and R. W. Heath Jr., "Capacity and Scaling Laws of Dense mmWave and Interference Alignment Ad Hoc Networks," in *Proc. of IEEE Military Communications Conference (MILCOM)*, Oct 2016.

[70] A. Thornburg and R. W. Heath Jr., "Ergodic Capacity in mmWave Ad Hoc Network with Imperfect Beam Alignment," *2015 IEEE Military Communications Conference (MILCOM)*, 2015.

[71] ——, "Capacity and Coverage in Clustered LOS mmWave Ad Hoc Networks," in *Proc. of IEEE Global Telecommunications Conference (GLOBECOM)*, Dec 2016.

[72] ——, "Ergodic Capacity of mmWave Ad Hoc Networks," *to appear in IEEE Trans. Wireless Commun.*, 2018.

[73] S. Ulukus, A. Yener, E. Erkip, O. Simeone, M. Zorzi, P. Grover, and K. Huang, "Energy harvesting wireless communications: A review of recent advances," *IEEE J. Sel. Areas Commun.*, vol. 33, no. 3, pp. 360–381, Mar. 2015.

[74] R. Vaze and R. Heath, "Transmission capacity of ad-hoc networks with multiple antennas using transmit stream adaptation and interference cancellation," *IEEE Trans. Inf. Theory*, vol. 58, no. 2, pp. 780–792, 2012.

[75] R. Vaze, K. Truong, S. Weber, and R. Heath, "Two-way transmission capacity of wireless ad-hoc networks," *IEEE Trans. Wireless Commun.*, vol. 10, no. 6, pp. 1966–1975, 2011.

[76] K. Venugopal, M. C. Valenti, and R. W. Heath, "Device-to-device millimeter wave communications: Interference, coverage, rate, and finite topologies," *IEEE Trans. Wireless Commun.*, vol. 15, no. 9, pp. 6175–6188, Sep. 2016.

[77] K. Venugopal, M. C. Valenti, and R. W. Heath Jr., "Device-to-Device Millimeter Wave Communications: Interference, Coverage, Rate, and Finite Topologies," *CoRR*, vol. abs/1506.07158, 2015. [Online]. Available: http://arxiv.org/abs/1506.07158

[78] L. Wang *et al.*, "Millimeter wave power transfer and information transmission," in *Proc. IEEE Global Commun. Conf.*, Dec 2015, pp. 1–6.

[79] S. Weber, J. Andrews, and N. Jindal, "An overview of the transmission capacity of wireless networks," *IEEE Trans. Commun.*, vol. 58, no. 12, pp. 3593–3604, 2010.

[80] J. Winters, "Smart antenna techniques and their application to wireless ad hoc networks," *IEEE Trans. Wireless Commun.*, vol. 13, no. 4, pp. 77–83, 2006.

[81] J. Yang, "Achievable rate for energy harvesting channel with finite blocklength," in *Proc. of IEEE Int. Symp. Inf. Theory*, Jun. 2014, pp. 811–815.

[82] A. Zanella, N. Bui, A. Castellani, L. Vangelista, and M. Zorzi, "Internet of things for smart cities," *IEEE Internet Things J.*, vol. 1, no. 1, pp. 22–32, Feb. 2014.